CONTACT METAMORPHISM AND METASOMATISM OF PALEOZOIC ROCKS NEAR STRONGHOLD CANYON, DRAGOON MOUNTAINS, ARIZONA

by

Jodi Ann Rushing

A Thesis Submitted to the Faculty of the

DEPARTMENT OF GEOSCIENCES

In Partial Fulfillment of the Requirements
For the Degree of

MASTER OF SCIENCE

In the Graduate College

THE UNIVERSITY OF ARIZONA

1 9 7 8

STATEMENT BY AUTHOR

This thesis has been submitted in partial fulfillment of requirements for an advanced degree at The University of Arizona and is deposited in the University Library to be made available to borrowers under rules of the Library.

Brief quotations from this thesis are allowable without special permission, provided that accurate acknowledgment of source is made. Requests for permission for extended quotation from or reproduction of this manuscript in whole or in part may be granted by the head of the major department or the Dean of the Graduate College when in his judgment the proposed use of the material is in the interests of scholarship. In all other instances, however, permission must be obtained from the author.

SIGNED: Jodi Rushing

APPROVAL BY THESIS DIRECTOR

This thesis has been approved on the date shown below:

R.E. Beane
R. E. BEANE
Associate Professor of Geosciences

11/22/78
Date

ACKNOWLEDGEMENTS

Dr. Richard Beane stimulated my graduate studies initially through his meticulous teaching of theories of ore deposition. I am indebted to him for introducing me to the study area, for editing the text, and for providing financial support. Most importantly, I have benefited from his sincere academic and moral support. I wish to acknowledge Drs. John Guilbert and Spencer Titley whose many economic geology field trips provided the impetus for choosing a field related thesis study. Dr. Guilbert further provided constructive criticism of the text. Several graduate students provided academic insights into various aspects of this study. Rick Preece's help with interpretation of fluid inclusion data, Doug Lane's instruction and assistance in obtaining microprobe analyses, and Bill Nieman's suggestions for evaluating the structural geology were invaluable. Finally, I acknowledge Lois Cantrell for spurring my interest in geology eleven years ago.

TABLE OF CONTENTS

TABLE OF CONTENTS--*Continued*

LIST OF ILLUSTRATIONS

LIST OF TABLES

ABSTRACT

Near the mouth of Stronghold Canyon in the Dragoon Mountains, rocks ranging in age between Precambrian and Middle Tertiary have been deformed during the Laramide and Middle Tertiary orogenies and mineralized during Middle Tertiary time. Laramide deformation is characterized by a major period of folding and low angle faulting, and Middle Tertiary deformation is characterized by a period of high angle faulting that accompanied and postdated the intrusion of Stronghold Granite.

The intrusion of Stronghold Granite provided the heat source for contact thermal metamorphism and pyrometasomatism of adjacent Paleozoic carbonate rocks. The deposition of metasomatic minerals including garnet, fluorite, magnetite, and base metal sulfides and their oxidation products postdates isochemical metamorphism of carbonate rocks and is localized almost exclusively along faults. Geochemical studies of two pyrometasomatic skarn assemblages indicate that they formed from solutions at temperatures between 300-500°C and salinities as high as 50 weight percent NaCl equivalent. Minimum pressures attending skarn formation were determined from fluid inclu-

sion studies to be between 100 and 680 bars. These minimum pressures correspond to depths of 1.0 to 8.8 km and 0.4 to 2.3 km assuming hydrostatic and lithostatic loads, respectively. Temperatures determined from calculated mineral stability fields for one skarn assemblage are in agreement with temperatures obtained from fluid inclusion studies.

INTRODUCTION

The Dragoon Mountains are a north-northwest trending range, 32 km long and 9 km wide, that lies within the Basin and Range province, 130 km southeast of Tucson, Arizona (Figure 1). The most comprehensive geologic study of the Dragoons was made by Gilluly (1956) who documented the geologic history of the entire range. Cederstrom (1946) emphasized the structural geology of the central Dragoons, and more recently, Keith and Barrett (1976) have reinterpreted the structural evolution of approximately the same area. Vein, pyrometasomatic, and irregular replacement deposits of copper, silver, zinc, lead, and iron occur throughout the Dragoon Mountains and are related to igneous activity assigned a Triassic-Jurrassic or Middle Tertiary age. Study of the ore and mineral deposits of the Dragoons is scant; it includes the early work of Ransome (1913) and Wilson (1927) at the Courtland-Gleeson district and the work of Sousa (in preparation) in Middlemarch Canyon. In the northeastern portion of the Dragoon Mountains (Figure 2), two plutonic rocks, Cochise Peak Quartz Monzonite and Stronghold Granite, are in contact with Paleozoic carbonate rocks which show effects of both initial widespread thermal metamorphism and subsequent local metasomatism with related sulfide

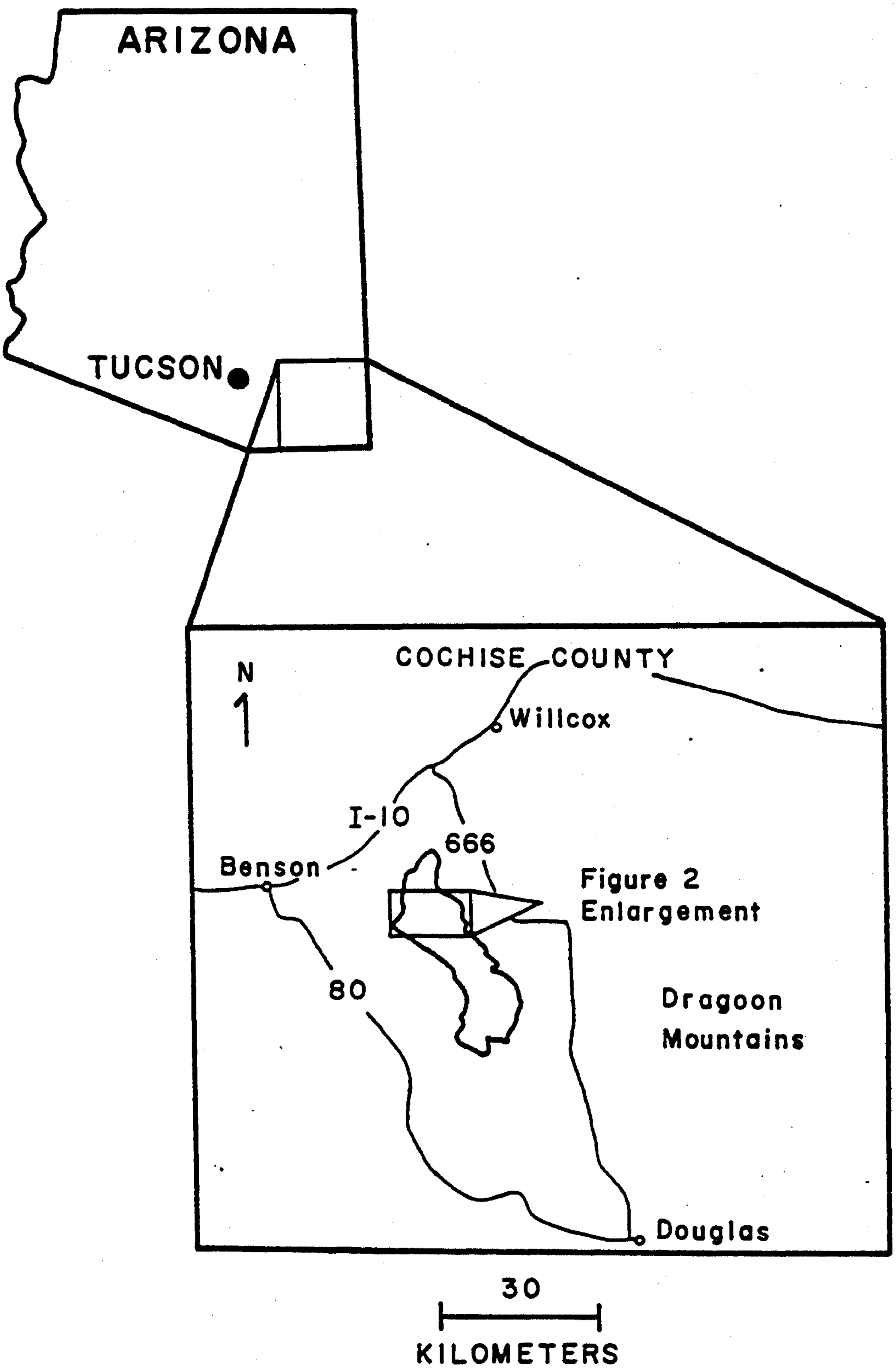

Figure 1. Location map of the Dragoon Mountains.

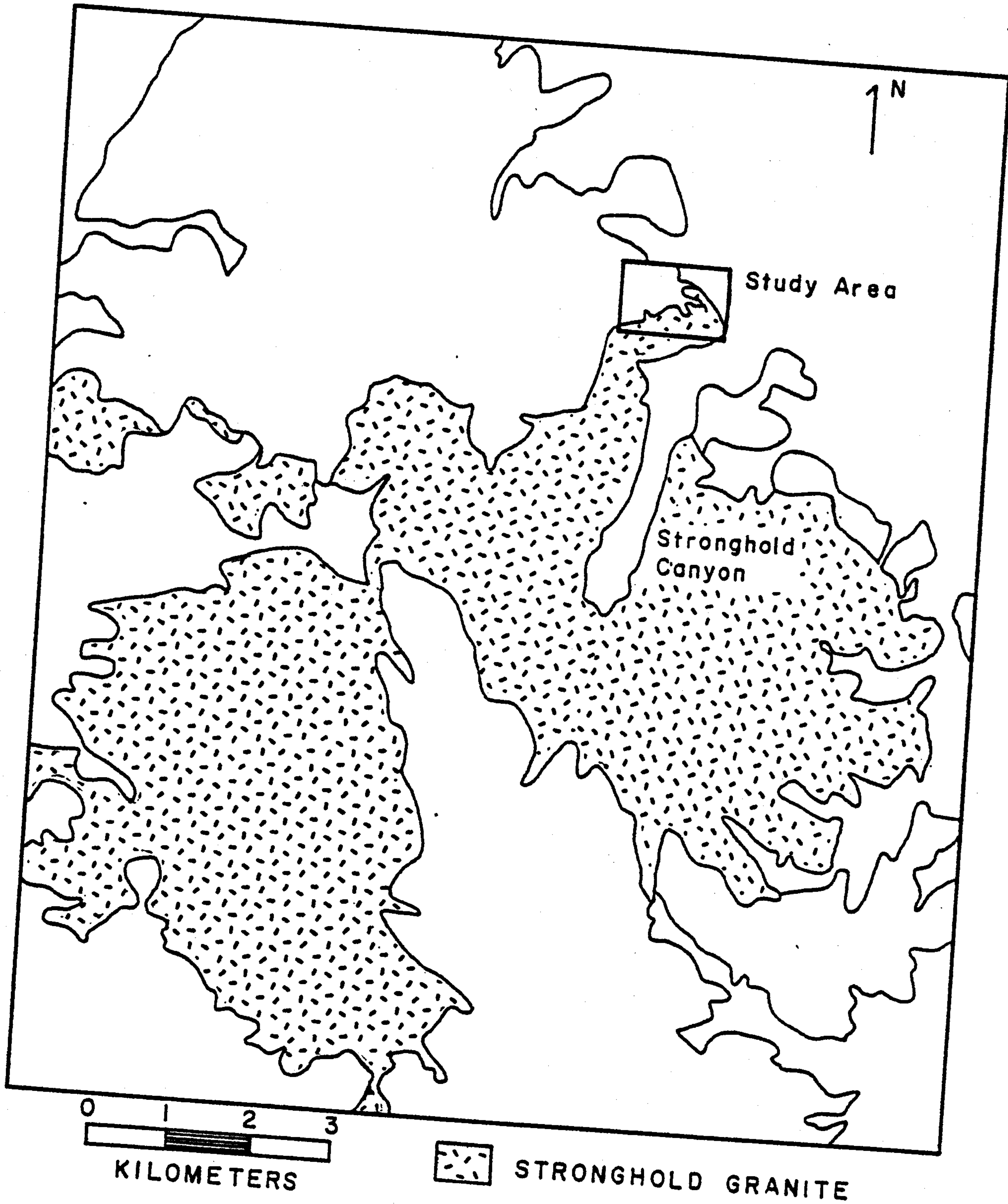

Figure 2. Location map of the study area at the north-eastern contact of the Stronghold Granite.

mineralization. The ages of Cochise Peak Quartz Monzonite and Stronghold Granite were determined through field mapping by Gilluly (1956) to be Jurassic and Middle Tertiary, respectively, and therefore, either or both plutons could have been the heat source for thermal metamorphism and metasomatism of adjacent Paleozoic rocks. However, according to Keith and Barrett (1976), Cochise Peak Quartz Monzonite is Precambrian in age which eliminates the quartz monzonite as a possible heat source for skarn formation in the Paleozoic rocks.

The purpose of this study is to examine in detail the geologic, mineralogic, and geochemical characteristics of two metasomatic skarn deposits in order to define their environments of formation. In order to determine the relative ages of plutonism, metamorphism, and metasomatism, as well as the geologic controls of mineralization, a geologic map was made of the study at a scale of 1:3780. Petrography, X-ray diffraction, and electron microprobe analyses provided data to identify minerals and determine their composition, and fluid inclusion studies were used to delimit temperature, pressure, and salinity ranges attending skarn formation. Finally, graphic representation of mineral stabilities was employed to show mineral paragenesis of one of the skarns.

LITHOLOGIC UNITS

Sedimentary Rocks

Sedimentary rocks in the Dragoon Mountains include approximately 1870 meters of Paleozoic shallow marine carbonates and shales and 5000 meters of Late Cretaceous conglomerate, sandstone, shale, and limestone, principally of the Bisbee Formation (Gilluly, 1956). Most of the contacts between formations are faults, making correlations difficult. Folding and metamorphism have further rendered the identification of formations ambiguous. However, several distinguishing characteristics described by Gilluly (1956) and Bryant (1968) were used to delineate formations in the area covered by this study.

Bolsa Quartzite

The Bolsa Quartzite, of Middle Cambrian age, is a light pink to white, medium grained and moderately well sorted quartzite and conglomeratic quartzite that contains $\leq$ 10% total feldspar + sericite + pyrite + iron oxides. The Bolsa is noted for its bold outcrop pattern and was mapped by recognition of its color, texture, and stratigraphic position. Cross bedding, typical of the Bolsa, was seen in only one outcrop, probably because most outcrops show strong cataclasis.

Brock and Engelder (1977) have demonstrated that the destruction of bedding in quartz arenite in structurally deformed areas may be the result of cataclasis. The maximum thickness of the Bolsa Quartzite in the study area is 25 meters. Thermal metamorphism and metasomatism have not significantly affected the quartzite. Iron oxide occurs as indigenous grains and as transported films along fractures. Sericite replaces feldspar and occurs as matrix material within outcrops of Bolsa that are deformed. In the field area, the lower Bolsa contact is a fault that juxtaposes quartzite against Cochise Peak Quartz Monzonite. The upper contact is poorly exposed and is interpreted as a fault between Bolsa Quartzite and Abrigo Formation.

Abrigo Formation

Gilluly (1956) termed the Abrigo Formation, of Middle to Late Cambrian age, the marker unit of the Dragoons, and indeed, it is the most distinctive, heterogeneous rock type in the map area. Characteristically, the Abrigo is composed of thin ($\leq$ 2 cm thick), alternating gnarly beds of limestone and fine clastics that form a ribbed weathered surface. Flat pebble conglomerates and moderately thick sequences of siltstone, shale, and limestone are also present. A maximum thickness of unfaulted Abrigo Formation, which occurs in the eastern portion of the area, is 100 meters. Thermal metamorphism of the Abrigo has enhanced the original compositional banding and layering of the rock.

Although no complete section of Abrigo is exposed in the area, it can be macroscopically divided into three units: hornfels, marble, and marble - garnetite (after Perry, 1964). The hornfels is a dense, banded or mottled, light blue to black rock whose color reflects a distinct mineralogic composition. The bands are composed of biotite, diopside, or garnet hronfels that are respectively black, blue, and green in color. Biotite and diopside hornfels are intergrown with equal amounts of quartz and K-feldspar. Textures vary between bands: in biotite bands, biotite is very fine grained and lineated; in diopside bands, diopside is medium to fine grained hornfelsic. The thin bedded white marbles are either pure or contain lenses of green and blue hornfels. In thin section, the marbles contain crystalloblastic calcite and varying amounts of epidote, diopside, wollastonite, and garnet. The more siliceous marbles also contain vesuvianite, scapolite, quartz, K-feldspar and minor plagioclase. The marble - garnetite member is characterized by its gnarly, ribbed outcrop pattern of resistant bands of green garnet hornfels and non-resistant bands of marble.

The lower contacts of the Abrigo are faults that juxtapose Pinal Schist, Cochise Peak Quartz Monzonite, and

Bolsa Quartzite with various lithologies of the Abrigo. The upper contact is typically a poorly defined, faulted or depositional contact with the Martin Formation.

Martin Formation

Typically, the Late Devonian Martin Formation is a thin to medium bedded, light grey to dark blue-grey, finely to medium crystalline limestone with a few interbedded sandstone units. In a few places, beds of fossil hash containing Atrypa brachiopods are present. Otherwise, the rock is distinguished by its light to yellow-brown, flaggy to rounded weathered surfaces. Silty and sandy members of the Martin were probably silicified during metamorphism while the carbonate layers macroscopically seem little affected. The maximum thickness of Martin Formation is 80 meters in the study area.

The lower contact of the Martin is most commonly a fault, but in the shallow syncline in the eastern portion of the study area, the Martin is possibly depositional on the Abrigo Formation. The upper contact, also a fault, is underlain by an iron stained, 0.5 meter thick sandstone bed, and by a low angle gouge zone delineated by a row of trees or by an abrupt change in lithology from fine grained grey-brown limestones of the Martin to the overlying massive, coarse grained white marbles of the Escabrosa Limestone.

Upper Paleozoic Rocks, Undifferentiated

The Early Mississippian Escabrosa Limestone, the Pennsylvanian Horquilla and Earp Formations, and the Early Permian Colina Limestone occur on the north and south sides of the prominent east - west trending ridge in the northwest portion of the map area. They were mapped together because they are relatively unaffected by metasomatism. Changing lithologies are evident, however, and scrutiny of the outcrops is necessary to distinguish these formations. On the south side of the aforementioned ridge, the Escabrosa Limestone and the Horquilla Formation are the only two Upper Paleozoic formations within the study area. The contact between the two, mapped as a major fault by Gilluly (1956), is evident only in the westernmost outcrops where a distinct structural discontinuity exists across the contact. Highly folded and contorted, cliff-forming chert and sandstone beds of the Horquilla Formation lie over essentially homoclinally dipping, more subdued outcrops of the Escabrosa Limestone. Further to the east, the contact appears gradational. The rocks of these two formations vary from massive, coarse grained white marble and fine grained grey limestone containing chert nodules, upsection to medium bedded, grey to dark grey limestone, bedded chert and light tan colored silicified sandstone. This gradation is also marked by both the occurrence of one meter thick beds of dark grey aphanitic, crinoidal limestone, noted by Gilluly (1956) to be characteristic of the uppermost Escabrosa, and the local occurrences of silty laminae.

On the north side of the east - west ridge, sections showing Escabrosa Limestone through Colina Limestone are exposed (Gilluly, 1956). The distinction between formations is extremely difficult because bedding plane orientations are highly variable and exposures are patchy. Gilluly (1956) admits the difficulty of distinguishing these lithologies where they have been thermally metamorphosed, as in this area. Generally, the pure Escabrosa Limestone is metamorphosed to coarse grained white marble, while chert nodules are often rimmed with or totally converted to wollastonite. Stratigraphically higher marblized beds are typically finer grained and darker than those of the Escabrosa and contain numerous interbedded silty laminae that are metamorphosed to green garnet. Metamorphism, however, is not persistently intense because fossils are locally abundant.

Igneous Rocks

Two major plutonic bodies outcrop in the map area: Cochise Peak Quartz Monzonite and Stronghold Granite. Generalized and detailed geologic maps (Figures 3, and 4 [in pocket]) show the relationships among the plutonic and

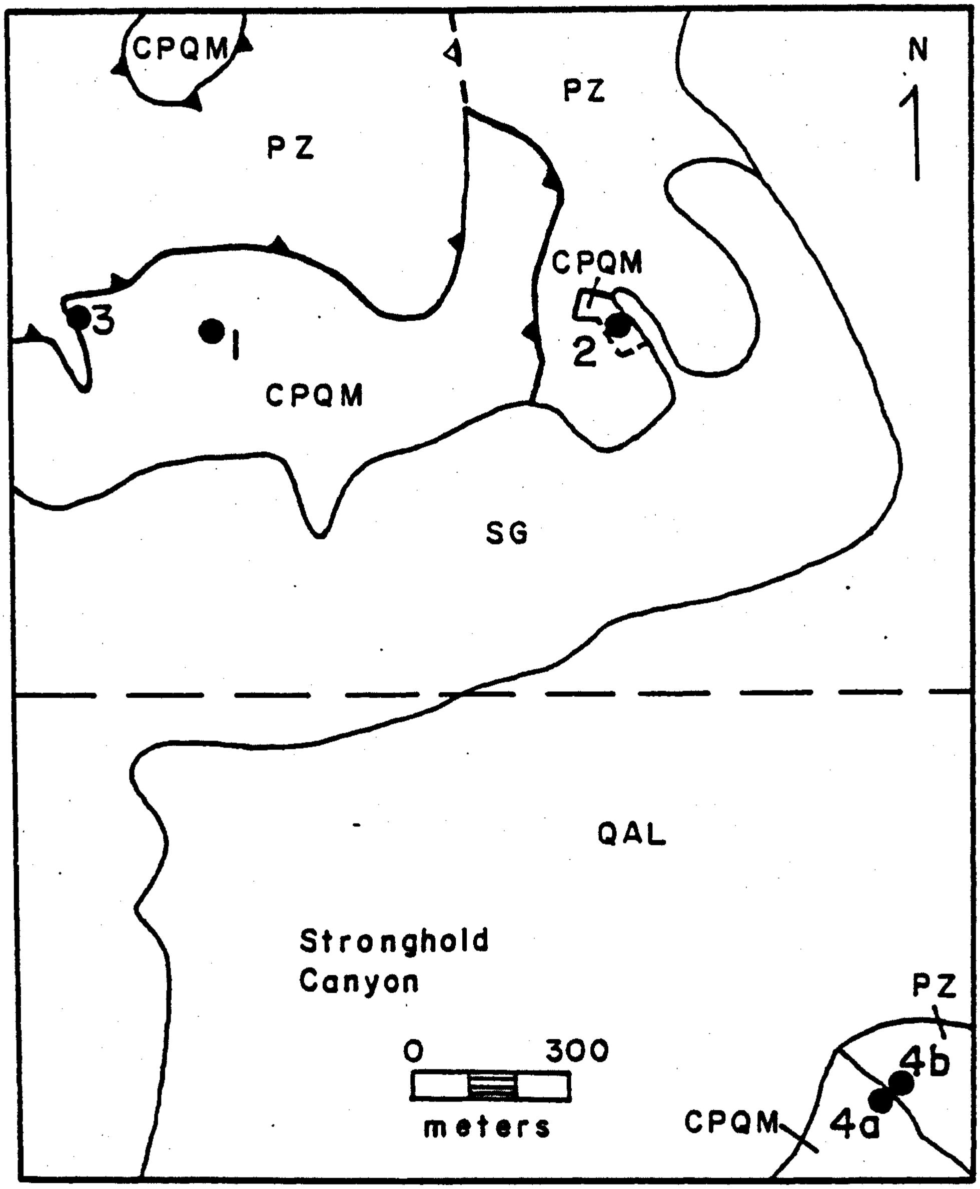

Figure 3. Generalized geologic map showing distribution and contacts of major rock types. -- CPQM, Cochise Peak Quartz Monzonite; PZ, Paleozoic sedimentary rocks; SG, Stronghold Granite; QAL, Quaternary alluvium. Numbers refer to sample locations of quartz monzonite described in text. Dashed line is the approximate southern boundary of the study area. See the detailed geologic map in Figure 4 for explanation of map symbols.

sedimentary rocks. One of the three areas of quartz monzonite referred to by Gilluly (1956, p. 63), near the mouth of Stronghold Canyon, outcrops in the study area. Two smaller outcrops of quartz monzonite are also present, one in the east-central and the other in the northwestern portion of the map area. Stronghold Granite, which outcrops over an area of 40 km^2, is the youngest major pluton in the Dragoon Mountains with determined ages of 22 ± 3 m.y. (Damon and Bickerman, 1964) and 25.9 ± 2 m.y. (Marvin and others, 1973). Its northeastern most exposure in the range occurs in the map area (Figure 2). The age of Cochise Peak Quartz Monzonite has been interpreted alternately as Jurassic (Gilluly, 1956) and Precambrian (Keith and Barrett, 1976), in the central Dragoon Mountains. The age of quartz monzonite relative to carbonate rocks is instrumental in deciphering its role in the thermal metamorphism and metasomatism of the carbonate rocks and separating these from similar effects by the Stronghold Granite.

Cochise Peak Quartz Monzonite

The major mass of Cochise Peak Quartz Monzonite is bounded by an intrusive contact of Stronghold Granite on the south and by fault contacts with Paleozoic rocks on the north, west, and east (Figure 3). No intrusive relationships exist between quartz monzonite and Lower Paleozoic rocks as mapped by Gilluly (1956). Instead, the quartz monzonite is variably faulted against rocks of the Bolsa Quartzite through Upper Paleozoic formations. In several places, the fault contacts are sharp and are characterized by shear foliation parallel to the fault. Where the contact is not visible, it is mapped between outcrops of quartz monzonite and Paleozoic rocks that were $\leq$ 5 meters apart.

Petrographic study was made of three distinct field occurrences of Cochise Peak Quartz Monzonite: 1) fresh appearing, 2) hydrothermally altered, and 3) shear foliated quartz monzonite, examples of which are shown as location numbers 1, 2, and 3, respectively (Figure 3). One additional occurrence outside of the map area (sample numbers 4a and 4b, Figure 3) was examined to determine the nature of the Bolsa Quartzite - Cochise Peak Quartz Monzonite contact where it has not been faulted.

The first, and characteristically the freshest, occurrence of quartz monzonite is represented by two samples from the center of the large outcrop of Cochise Peak Quartz Monzonite (Location 1, Figure 3). In hand specimen, the rock is typically a greenish grey, porphyritic quartz monzonite that weathers to rust-colored hummocky and grusy masses. Porphyritic texture is discernible by the 2 cm by 1 cm flesh colored microcline phenocrysts that constitute 10% of the rock. Where the rock is altered, its identification is ascertained by ghost outlines of these phenocrysts. In thin section, slightly altered microcline phenocrysts contain sericitized plagioclase and chlorite inclusions. The groundmass consists of small grains, $\leq$ 2 mm in diameter, of quartz (30-35%), plagioclase (30-35%), K-feldspar (15%), and biotite (5%). Although largely obliterated by sercitization, albite twinning in a few plagioclase grains and gridiron twinning in K-feldspar are suggested by vague extinction patterns. Biotite grains are moderately altered to chlorite and iron oxides; intergrown with biotite are a few coarse muscovite grains. Accessory minerals include magnetite and zircon. A chemical analysis of Cochise Peak Quartz Monzonite is given by Gilluly (1956, p. 65), and he notes that the low potash content is probably a result of a biased sample, namely one with a low phenocryst population, which may not represent the bulk composition of the rock.

Locally, the quartz monzonite is cut by near vertical sericite veinlets trending N65-80W and N20W which are approximately 1 mm wide and spaced at intervals usually < 15 cm. Breakage along these veinlets reveals a face of shiny coarse muscovite. Petrographically, this rock is distinguished from the unveined quartz monzonite by increased sericitization of both phenocrysts and matrix. A few plagioclase grains show intense alteration to sericite, biotite, and epidote (?) with no preservation of relict texture except for habit. The veinlets are composed of euhedral muscovite grains plus or minus quartz and minor fluorite. Alteration halos $\leq$ 1 cm wide consist of minute, seed-like grains of sericite and quartz.

The two samples studied display a crystalloblastic-cataclastic texture. Quartz grains show undulatory extinction; grain boundaries are crushed or recrystallized. Quartz and feldspars are fractured, and phyllosilicate plates are bent, but intense crushing was not observed.

The second group of quartz monzonite samples (Location 2, Figure 3) were from a small outcrop that is separated from a pyrometasomatic skarn (skarn A in a later discussion) by a dike of Stronghold Granite. In hand specimen, this rock is characterized by coalescing sericite veinlets spaced $\leq$ 2 cm apart, giving the rock a bleached appearance, and by a knotty texture imparted by clusters of quartz grains that stand in relief. In thin section, the rock is strongly altered. Round clusters of quartz grains (~20%) exhibiting various degrees of fracturing are surrounded and impregnated by fine grained masses of quartz (30%), sericite (40%), and andalusite plus biotite (5-8%). Feldspars are replaced by sericite and quartz, and sericite is, in turn, replaced by andalusite, biotite, and quartz. Virtually no feldspar remains in the rock, but its original presence is indicated by ill-defined rectangular clusters of andalusite, quartz, sericite, and biotite. Accessory magnetite and zircon commonly occur with biotite; no chlorite is present. Sericite veinlets have similar mineralogies and alteration halos as those described from the fresh appearing quartz monzonite. Individual specimens of quartz monzonite containing sericite veinlets differ in density of veining. Proximity of quartz monzonite to granite is not the controlling factor responsible for the pervasive veining because elsewhere, as described below, quartz monzonite in contact with granite does not show these alteration effects. Instead, pre-alteration fracturing of the quartz monzonite is probably responsible for the more abundant alteration in this area.

The third distinct field occurrence of quartz monzonite (Location 3, Figure 3) is along and near the fault contact with Paleozoic rocks. Macroscopically, the rock shows cataclastic deformation whereby a shear foliation has obliterated its characteristic porphyritic texture and imparted a flattened texture to the rock. No minerals are discernible in hand specimen, but microscopically, this shear foliation is manifested as lens-shaped 'eyes' composed of quartz and feldspar which are surrounded by irregular black bands of finely granulated matrix of the same minerals plus chlorite.

One sample of quartz monzonite was taken from an 8 cm wide zone of dark grey mylonite sandwiched between foliated quartz monzonite and relatively undeformed Abrigo Formation. In thin section, quartz, chlorite and minor calcite are more finely comminuted than the cataclastites described above. Such strong shearing is a local feature near the fault; elsewhere, quartz monzonite is only moderately deformed and retains a distinct shear foliation.

A fourth occurrence of quartz monzonite (Locations 4a and 4b, Figure 3), outside of the field area, was studied to determine its contact relationship with Bolsa Quartzite which Gilluly (1956) mapped as intrusive. One sample each of quartz monzonite (4a) and quartzite (4b) separated by a distance of 3 meters were examined. The quartz monzonite consists of aggregates of quartz grains and slightly sericitized K-feldspar phenocrysts that compose approximately 80% of the rock and that are engulfed in a matrix of sericite. Single K-feldspar phenocrysts have been broken into smaller grains and grain boundaries are subrounded to subangular; they are not shattered or crushed, but appear eroded. Iron oxides, leucoxene, and chlorite constitute < 2% of the rock. The sample of Bolsa Quartzite mimics the mineralogy of the quartz monzonite, except that the former lacks sericite and mafic minerals. Subrounded to rounded clasts of quartz and quartz plus feldspar, which are comparable in size to the quartz-feldspar aggregates in the adjacent quartz monzonite, form the bulk of this arkosic conglomeratic unit of the Bolsa. The presence of eroded K-feldspar clasts, 2 cm by 1 cm in size, in the arkose suggests that their source is the quartz monzonite. Field observations corroborate the petrographic interpretation that Bolsa Quartzite is depositional upon Cochise Peak Quartz Monzonite at this locality.

Stronghold Granite and Aplite Dikes

The Stronghold Granite, which outcrops in the southern portion of the map area (Figure 3), constitutes a small segment of the northeastern contact of Stronghold Granite which makes up the large bulging mass in the Dragoon Mountains (Figure 2). The granite forms one continuous body in the southern half of the study area from which two parallel dike-like lobes extend N 55 W for approximately 400 meters; these serve to confine older rocks as roof pendants in the granite. The outcrop pattern of Stronghold Granite is distinct; fins and rounded boulders of granite result from weathering along four major joint sets:

1) N 35 W, 66 SW,
2) N 60-70 E, 85 SE,
3) N 7 W, 75 NE - 76 SW to N 11 E, 80 NW, and
4) N 75 W, 40 NE.

Measured fracture densities in the area average, respectively, 9, 6, 5, and 3 fractures per meter.

In the study area, the Stronghold Granite intrudes, along much of its contact length, Cochise Peak Quartz Monzonite (Figures 3 and 4). Generally, the contact is sharp and dips toward the quartz monzonite, but a narrow zone of mixed rock is present where closely spaced aplite dikes approach the contact. Xenoliths and schlieren of quartz monzonite in granite are common. A narrow margin, < 20 cm wide, of recrystallized quartz monzonite occurs locally along the contact and is characterized by 1) the presence of secondary biotite whose shiny euhedral plates are distinguished from the stringy biotite in unrecrystallized quartz monzonite, and 2) the absence of K-feldspar phenocrysts. The alteration of quartz monzonite by granite is confined to this reaction selvage and widely spaced muscovite veinlets which were described earlier.

Petrographic description of the border phase of Stronghold Granite by Gilluly (1956) and Perry (1964) are corroborated here. The granite is a light grey, fine grained, slightly porphyritic biotite granite that weathers to a light yellow-brown friable mass. Phenocrysts of microcline and quartz are set in a matrix of the same plus oligoclase and biotite (≤ 5%); zircon and apatite are accessory minerals. Microcline is altered to sericite along cleavage planes, but overall, the granite notably lacks significant hydrothermal alteration; niether is there any development of endoskarn along its contact with sedimentary rocks.

Numerous N 15 - 20 W and a few N 50 W trending aplite dikes with near vertical dips extend as apophyses from the granite. The aplites are distinguished from the granite by their white color, saccharoidal texture, and diminished biotite content ($\leq$ 1%). As in the granite, the aplite is slightly porphyritic with quartz and microcline phenocrysts in a groundmass of the same, plus oligoclase. The feldspars show only minor alteration to sericite. The contacts between aplite and granite are gradational suggesting that they are cogenetic. In contrast, the contacts between aplite and older rocks are sharp, steeply-dipping contacts.

Rhyolite and Lamprophyre Dikes

Two north-northwest trending rhyolite dikes cut across the Stronghold Granite. The contact between rhyolite and granite is everywhere a 6 to 10 cm chilled margin in the dikes indicating that the rhyolite was intruded into relatively cold rocks. The rhyolite is a light pinkish-brown, hypidiomorphic porphyritic rock. In thin section, phenocrysts of orthoclase and quartz are set in a matrix of fine grained quartz, orthoclase, and zoned plagioclase. Radiating clusters of tridymite + K-feldspar (?) which surround slightly embayed hexagonal quartz grains indicate quenching. Minor biotite, which often appears to replace an unidentified acicular mineral, shows progressive replacement by magnetite. In addition, magnetite occurs as discrete cubic grains and along microfractures. Accessory zircon is also present. The feldspars are generally moderately altered to clays, but like the Stronghold Granite and aplite, the rock has not suffered significant hydrothermal alteration.

A few small lamprophyre dikes, interpreted by Gilluly (1956) to be Middle Tertiary in age, occur along or near faults in the Paleozoic rocks. The lamprophyre, which is fine grained and dark green to dark grey, is composed of hornblende plus plagioclase. One lamprophyre still occurs in a drainage along a fault between Cochise Peak Quartz Monzonite and Abrigo Formation. It is noted for the presence of 2 cm long, radiating actinolite crystals that occur along fractures in the lamprophyre.

Metamorphic Rocks

Three types of metamorphism represented in the study area are Precambrian dynamic metamorphism, Tertiary contact metamorphism, and metasomatism. Dynamically metamorphosed rocks are represented by the Precambrian Pinal Schist which outcrops in the northeastern portion of the study area and whose foliation trends north-northwest to northwest and dips 36° to 90° to the southwest. Subparallel to the foliation is an intruded arm of Stronghold Granite which divides the outcrop into two areas. Typically, the rock is a green-brown spotted schist. In thin section, the schistosity is defined by kink-folded laminae of muscovite and quartz; the green spots are rectangular to ovoid patches of muscovite discolored by iron oxide and irregularly rimmed by chlorite. The Pinal Schist is not mineralized and will not be discussed further.

Contact metamorphism and metasomatism occurring throughout most of the Paleozoic rocks in the study area are attributed to intrusion of Stronghold Granite.

Thermal Metamorphism

The degree of thermal metamorphism in the area is seen to depend on original mineraology and proximity of a heat source. Pure sandstone and limestone are converted to quartzite and marble, respectively, while impure rocks are metamorphosed to a more complex mineralogy of calc-silicates, feldspar, biotite, quartz, and calcite. The Abrigo Formation clearly displays the influence of original mineralogy on metamorphic products because its original compositional layering is preserved as distinct bands of metamorphic minerals. Interbands are composed of alternating biotite and diopside hornfels, or garnet hornfels and marble, and represent rocks that were originally shales and limey siltstones, or silty limestones and limestones respectively. Other metamorphic minerals such as wollastonite, vesuvianite, epidote, and scapolite also occur within these rocks.

Thermal metamorphism of the carbonate rocks also depends on the proximity of Stronghold Granite. The characteristics of the pluton (Gilluly, 1956) indicate that it is an epizonal pluton. Therefore, at a regional scale, the contacts of the pluton must be steep, but at a local scale, the granite appears to dip shallowly beneath older rocks. However, in the rocks furthest from Stronghold Granite in the study area (approximately 500 meters away from the granite contact), metamorphism has neither destroyed fossils nor converted chert nodules in limestone to wollastonite. These observations indicate decreasing metamorphism away from a steepened intrusive contact of Stronghold Granite.

Metasomatism

Metasomatic skarn assemblages consisting of garnet, iron oxides, and minor sulfides replace thermally metamorphosed rocks. The skarns are localized in highly fractured rocks, along faults, and in one case, near a dike of Stronghold Granite. Several skarns notably occur along the low angle fault between Cochise Peak Quartz Monzonite and Paleozoic rocks indicating that metamorphism post dated faulting, and thus, post dated emplacement of quartz monzonite. Two distinct skarns (skarns A and B in a later discussion) which contain respectively garnet + quartz + magnetite + fluorite and diopside + vesuvianite + calcite + muscovite were studied in detail to determine their environment of formation.

STRUCTURAL GEOLOGY

The structural geology of the area is complex, and is dominated by small and large scale folding plus at least two distinct periods of faulting. Small scale folds, which were not studied in detail here, are best displayed in the Abrigo Formation where ductility contrasts are developed in accordance with compositional layering. Figure 5 is a generalized geologic map showing the major structures in the study area.

One dominant structure in the area is an east-northeast vergent overturned anticline, evident from the relationships between Paleozoic stratigraphy and a major north to northwest trending low angle fault that cuts the Paleozoic rocks (Line AB, Figure 5). Figure 6 is a generalized cross section showing these relationships. Because the dip of the fault is less than that of bedding in the Abrigo Formation, and because Bolsa Quartzite and Cochise Peak Quartz Monzonite are faulted over the Abrigo, the Abrigo and Bolsa must be overturned. Therefore, the core of the anticline is Cochise Peak Quartz Monzonite which appears to have been thrust over the Abrigo Formation. The geometry and stratigraphic positions of units within the fold imply a

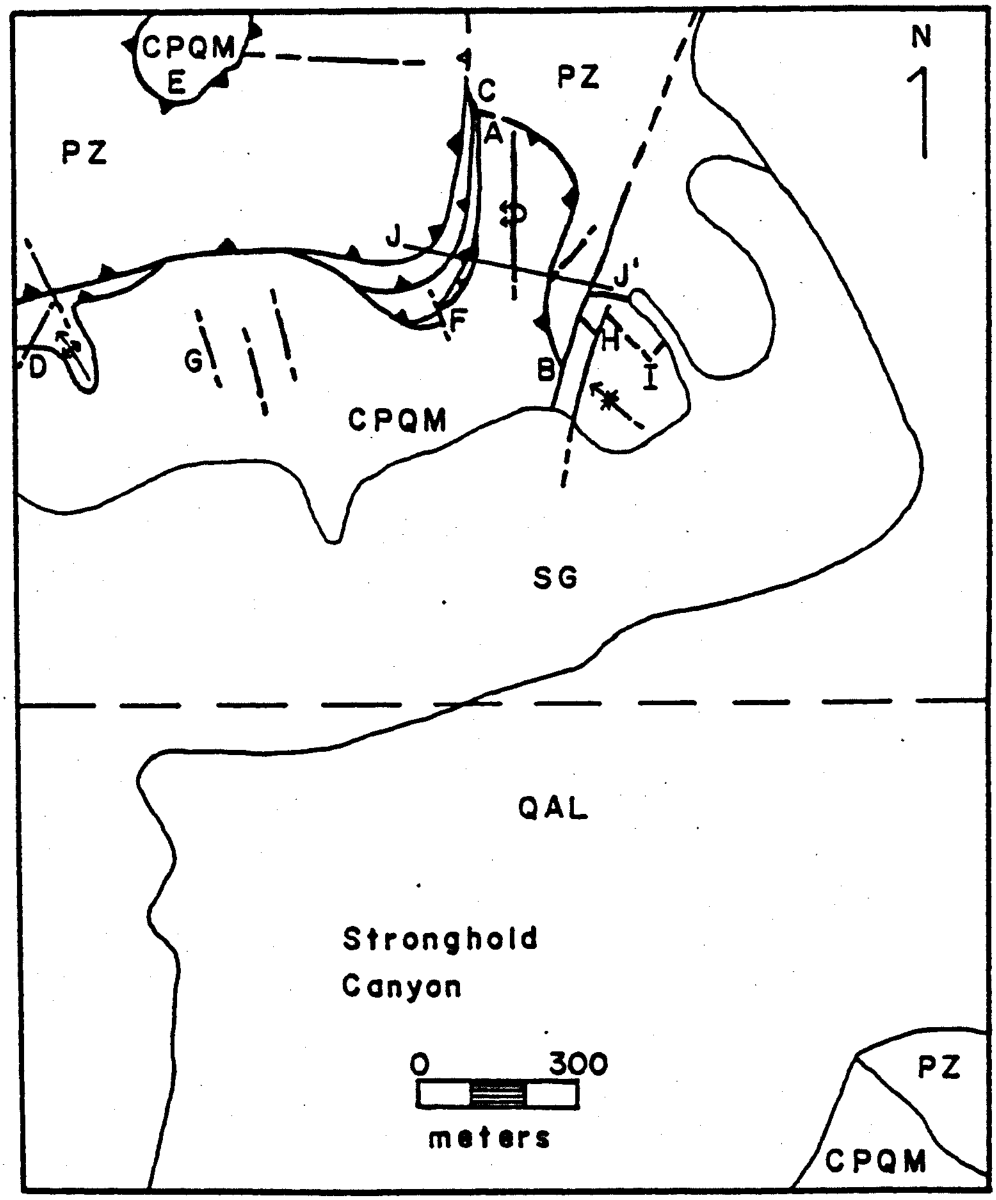

Figure 5. Generalized geologic map showing the major structures in the study area. -- Structure symbols are described in Figure 4; rock units are the same as those in Figure 3. Lettered localities refer to specific structures discussed in text. JJ' refers to the cross-section in Figure 6. Dashed line is the approximate southern boundary of the study area.

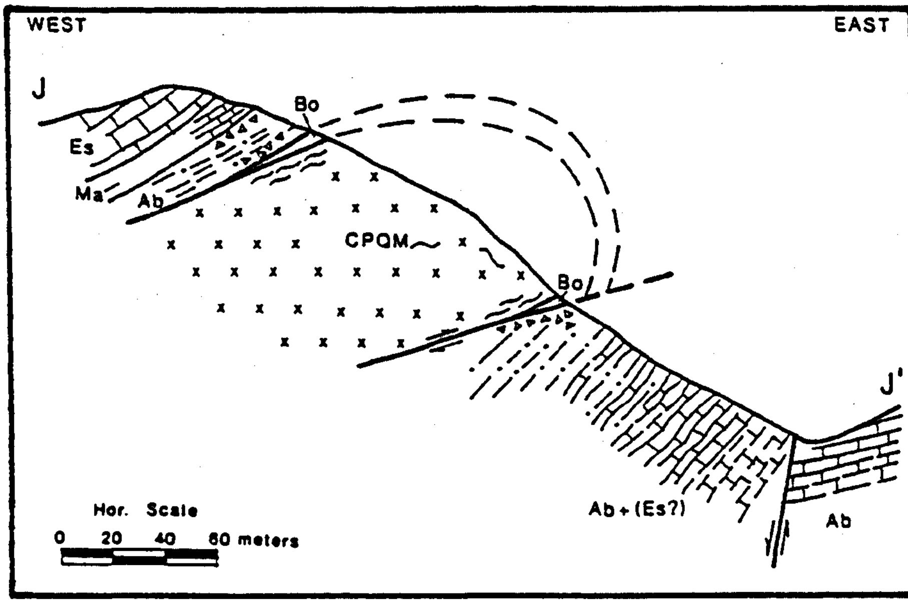

Figure 6. Schematic cross-section showing major overturned fold in the study area. -- Units are: CPQM, Cochise Peak Quartz Monzonite; Bo, Bolsa Quartzite; Ab, Abrigo Formation; Ma, Martin Formation; Es, Escabrosa Limestone. JJ' refers to the section line in Figure 5.

Precambrian age for the quartz monzonite. Similar fold-fault geometries are documented in the Wyoming Province of the Laramide Rocky Mountain foreland by Berg (1962).

Two smaller folds, a northwest plunging syncline and a northwest plunging anticline with satellite folds, occur respectively in the east and west portions of the area (Figures 4 and 5). Their trends are subparallel to the trend of the overturned fold suggesting that they were formed during the same period of folding. The most conspicuous large scale folds are displayed by the silicified layers of the Horquilla Formation that uphold the highest peaks in the study area. The folds appear to be asymmetric to the southwest which is different from the northeast sense of vergence of the overturned anticline. Paleozoic rocks, up to and including the Early Permian Colina Limestone, are involved in the folding, while Middle Tertiary aplite dikes cut the folds indicating maximum and minimum ages of folding.

Faults in the area were studied in detail because they often serve as loci to mineralization. The older, low angle faults are discussed in two groups: one, containing the north-northwest trending fault, occurs in the center of the map area, and the other, containing a set of northeast trending faults, is located in the central portion of the area (Figure 5). The north-northwest trending fault dips $< 44^{\circ}$ and generally $< 35^{\circ}$ to the southwest and juxtaposes

Cochise Peak Quartz Monzonite plus or minus Bolsa Quartzite upon Abrigo Formation in the overturned anticline discussed earlier. Several slivers of Bolsa, unmappable at a scale of 1" = 315', appear to be in the hanging wall of the fault; however, displacement along the contact between quartz monzonite and quartzite has also probably occurred. As the fault is approached, the rocks become increasingly crushed, as is documented in the field and in thin section. Six thin sections of quartz monzonite, Bolsa Quartzite, and hornfelsed Abrigo limestone show flattened fragments composed of minerals characteristic of each rock type that are engulfed by black bands of finely granulated matrix whose exact mineralogy could not be determined. The timing of this period of low angle faulting and thermal metamorphism cannot be unequivocally established from these thin sections. However, Gilluly (1956, p. 106) states that "thermal metamorphism due to this intrusion (i.e., Stronghold Granite) is superposed on the thrust breccias and transgresses major fault surfaces" indicating that metamorphism is Middle Tertiary in age and thus younger than low angle faulting.

This north-northeast trending low angle fault is cut by a fault of the second group of low angle faults which occur between Cochise Peak Quartz Monzonite and Paleozoic rocks and within Paleozoic rocks (Figure 5). The longest of these faults (Line CD, Figure 5), separating igneous and sedimentary rocks, is easily traced along its length except in the far west where it is inferred to lie beneath a large outcrop of Bolsa Quartzite. Scattered along this fault are several prospect pits containing calc-silicate, iron oxide, and sulfide mineralization.

The position of the skarns next to Cochise Peak Quartz Monzonite suggests that it was the heat source for skarn formation. However, mineralization is localized by the fault which only fortuitously is adjacent to the quartz monzonite. Sympathetic to this fault are a series of faults in an upright section of Paleozoic rocks. They are noted for their stacked, bedding plane character and the pinch and swell effect they have on outcrop patterns.

One additional low angle fault bounds a window of quartz monzonite in the northwest study area (Figure 4 and Location E, Figure 5). An attitude along the fault trending N 28 E and dipping 35° to the southeast was determined in one prospect pit where marbles of the Upper Paleozoic rocks form the hanging wall and quartz monzonite the footwall. Elsewhere, the fault is not visible, but its trace is thought to lie near slivers of Bolsa Quartzite that occur sporadically around the margins of, and never more than 2 meters away from, outcropping quartz monzonite. Two additional slivers of Bolsa Quartzite lie within the boundaries of the fault suggesting that they are erosional remnants of a once continous sheet of Bolsa that has since been detached from the quartz monzonite.

High angle faults, which are younger than the low angle faults, have two distinct trends: N 25 - 35 W and N 20 - 45 E. The faults formed during and after crystallization of Stronghold Granite as is indicated by 1) the orientation of aplite and rhyolite dikes that parallel these trends and 2) by two faults that cut the granite. One high angle fault, as well as an aplite dike, cut one of the low angle faults in the center of the area (Location F, Figure 5). At this location, the Bolsa Quartzite is offset approximately 15 meters. The high angle faults, like the low angle faults, served as loci to calc-silicate, iron oxide, and sulfide mineralization suggesting that mineralization occurred along both low and high angle faults during one event. Several N 25 W trending faults occur in the large outcrop of quartz monzonite (Location G, Figure 5); they are recognized by associated iron oxide staining and the presence of pyrite.

Two other inferred faults, one between Cochise Peak Quartz Monzonite and Abrigo Formation (Line HI, Figure 5) and the other between Pinal Schist and Abrigo Formation (Figure 4) are cut by Stronghold Granite and a rhyolite dike thereby giving a maximum and minimum age of formation of the faults. The northwest trends of the two faults are subparallel to the major folds suggesting that they formed at the same time as folding. In addition, the presence of numerous small fault blocks and folds, and structures larger than the scale of the map, are indicated by bedding plane orientations, but these were not studied because they do not appear related to mineralization.

In summary, it appears that folding of Paleozoic rocks in the area was accomplished by detachment from a basement of quartz monzonite during which tectonic thinning of sedimentary units and local shearing of the quartz monzonite occurred. Two periods of low angle faulting are suggested by crosscutting relationships. The attitude of the north-northwest trending low angle fault and the vergence of the overturned anticline suggest northeast transport of Paleozoic rocks. The transport direction of the younger northeast trending low angle faults is not known. The maximum and minimum ages of this period of deformation are Early Pennsylvanian and Middle Tertiary, which regionally can be correlated to Gilluly's (1956) Laramide (post Comanche to pre Middle Tertiary) period of deformation. Middle Tertiary high angle faulting accompanies and post dates intrusion of Stronghold Granite.

MINERALIZATION, ALTERATION AND METASOMATISM

Most skarn assemblages in the study area contain calc-silicates (chiefly garnet), iron oxides, and base metal sulfides and their oxidation products. Two skarns (Locations A and B, Figure 7) were studied in detail because they exhibited different characteristics from the majority of skarns in the study area. Skarn A was studied because it contains a distinct mineralogy of garnet + magnetite + fluorite, and skarn B was studied because it contains a simple mineralogy. Petrographic study served to establish stable mineral assemblages, paragenetic sequences and the role of fracturing during mineralization. Exact compositions of a few minerals were determined by electron microprobe analyses. The analyses were carried out to provide compositional data for use in mineral stability relations. Microprobe analyses are listed in Appendix A.

Skarn A

The assemblage garnet + magnetite + fluorite, making up skarn type A, occurs in an area 10 by 15 meters within a roof pendant of Abrigo Formation (Location A, Figure 7, and Figure 8). The outcrop pattern of Stronghold Granite around

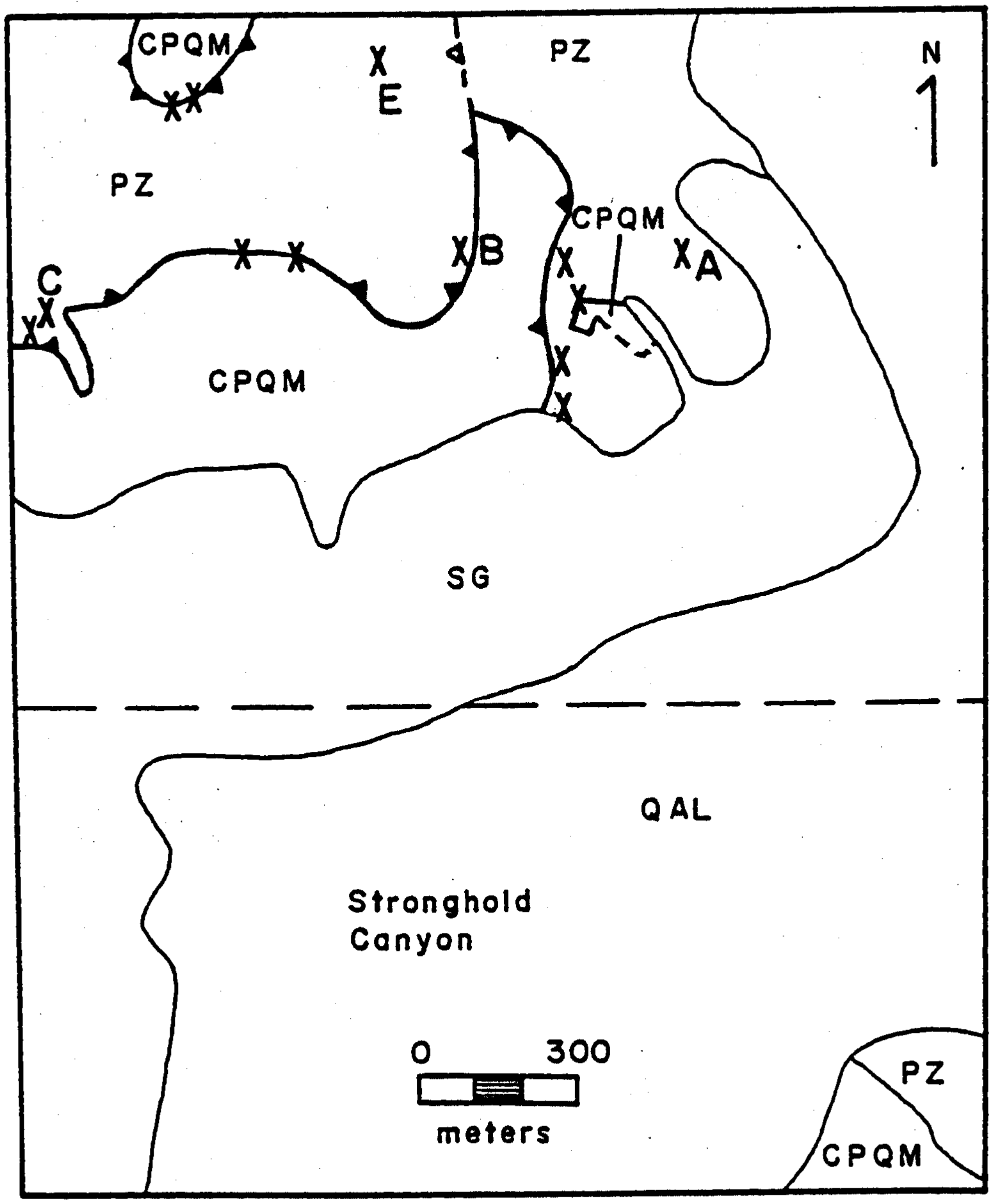

Figure 7. Generalized geologic map showing the locations of skarns in the study area. -- Lettered skarns refer to those discussed in text. See Figures 3 and 5 for description of map symbols. Dashed line is the approximate southern boundary of the study area.

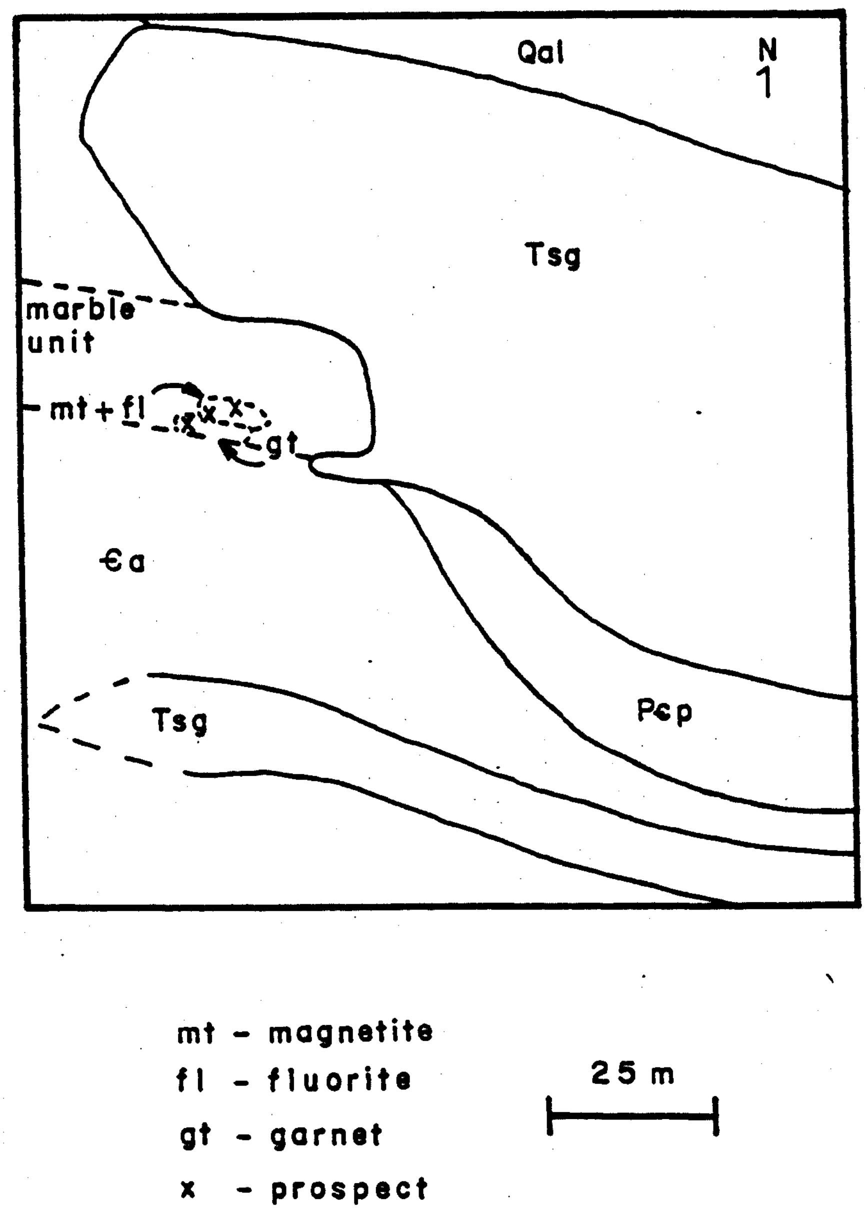

Figure 8. Sketch map showing the location of skarn A in a marble unit of the Abrigo Formation. -- Note that the Abrigo occurs as a roof pendant in Stronghold Granite. Note also that the skarn is composed of two distinct bodies, a garnet body and a magnetite + fluorite body, whose outlines are shown as short dashed lines.

the skarn suggests a nearby contact of granite with skarn although the two are not in visible contact at the surface. Two distinct parallel mineral bodies, one containing finely convoluted interbands approximately 3 mm thick of magnetite and fluorite, and the other consisting of garnet, strike N 80 W. The host for the metasomatic skarn is thermally metamorphosed Abrigo limestone.

Five samples of Abrigo limestone taken along strike of the skarn were studied in thin section. Figure 9 shows the paragenesis of the host rock minerals in relationship to deposition of metasomatic garnet. The host rock is composed predominantly of either calcite or interbanded calcite and calc-silicates. Crystalloblastic calcite contains interstitial poikiloblastic epidote and diopside. Locally, bladed wollastonite appears to grow out of the calcite, replacing calcite and diopside. Calc-silicate bands are composed predominantly, in order of decreasing abundance, of one or two of the following minerals: garnet, vesuvianite, scapolite, epidote, calcite, diopside, and quartz, all of which show varying degrees of alteration. Epidote and diopside, occurring as early minerals with calcite, are strongly pitted, cracked, and coated with a fine grained clay or limonite. Zoned, euhedral vesuvianite grains replace calcite, but have, in turn, been cut by a swarm of late calcite microveinlets and locally resorbed along vesuvianite - calcite grain

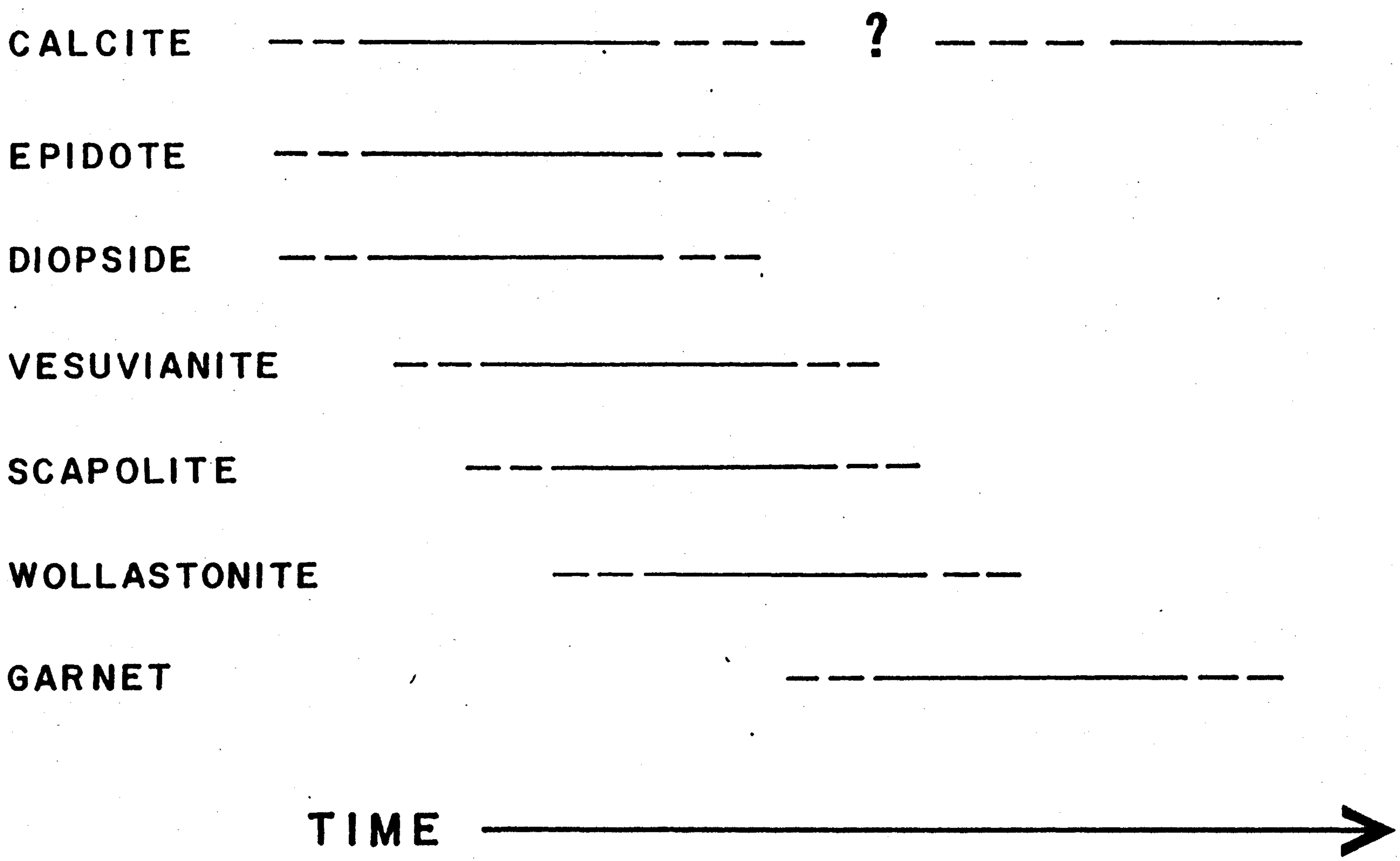

Figure 9. Paragenetic sequence of early skarn minerals in the Abrigo limestone host rock of skarn A. -- Garnet deposition marks the onset of Fe metasomatism in skarn A.

boundaries. Scapolite occurs as short, curved fibrous masses that replace vesuvianite and are invariably rimmed with iron oxide. The identity of the scapolite in thin section was confirmed by x-ray analysis to be predominately marialite. Radiating blades of wollastonite replace scapolite, calcite, and vesuvianite; the blades show little alteration. Microveinlets of calcite and iron oxide cut all of the calc-silicates of the host rock and impart a dirty appearance to them.

Irregular lenses of massive, isotropic garnet and a few zoned, sector twinned garnet crystals incompletely replace all of the above minerals except the late calcite and iron oxide. One microprobe analysis (Sample 49, Appendix A) shows that the replacement garnet is andraditic containing 0.56 mole fraction of andradite (X_{ad}) in the ugrandite solid solution series. Continual replacement of the host rock resulted locally in the total conversion of the host rock to andraditic garnet. Analyses of the garnet from the massive garnet body indicate compositions containing 0.65 to 0.86 mole fraction andradite. Magnetite and fluorite also cut the calc-silicates of the host rock (discussed in detail later), but without the more diffuse replacement exhibited by garnet.

In summary, an early stage of banded calc-silicate and marble formation, whose texture and mineralogy is probably inherited from compositional banding of the original sedimentary rock, has been overprinted by the deposition of Fe-rich garnet, magnetite, and fluorite. These relationships suggest an early period of thermal metamorphism of the Abrigo limestone altered by a later period of Fe metasomatism.

Petrographic Description of Skarn Minerals

The following paragraphs sequentially discuss the petrography of minerals listed in order of their relative abundance in skarn A. The paragenetic sequence of minerals in skarn A is depicted in Figure 10.

Garnet. Garnet, constituting up to 90% of the rock in the garnet body of skarn A, is dark green to brown and massive to slightly granular. In thin section, an interlocking network of euhedral crystals, $\leq$ 3 mm in diameter, display concentric zoning and sector twinning. Isotropic to slightly anisotropic cores with anisotropic overgrowth zones, indicated by zonal variation in birefringence and zonal distribution of alteration, are common. Interference colors vary between first order grey and first order yellow within the overgrowth zones. Milky quartz, making up ~ 3% of the skarn, was deposited after the garnet in interstitial vugs and fractures in the garnet.

Fluorite. Two distinct occurrences of fluorite indicate that it was deposited during two periods referred to as early and late. Early clear to purple fluorite occurs interbanded with magnetite, and late clear fluorite occurs as

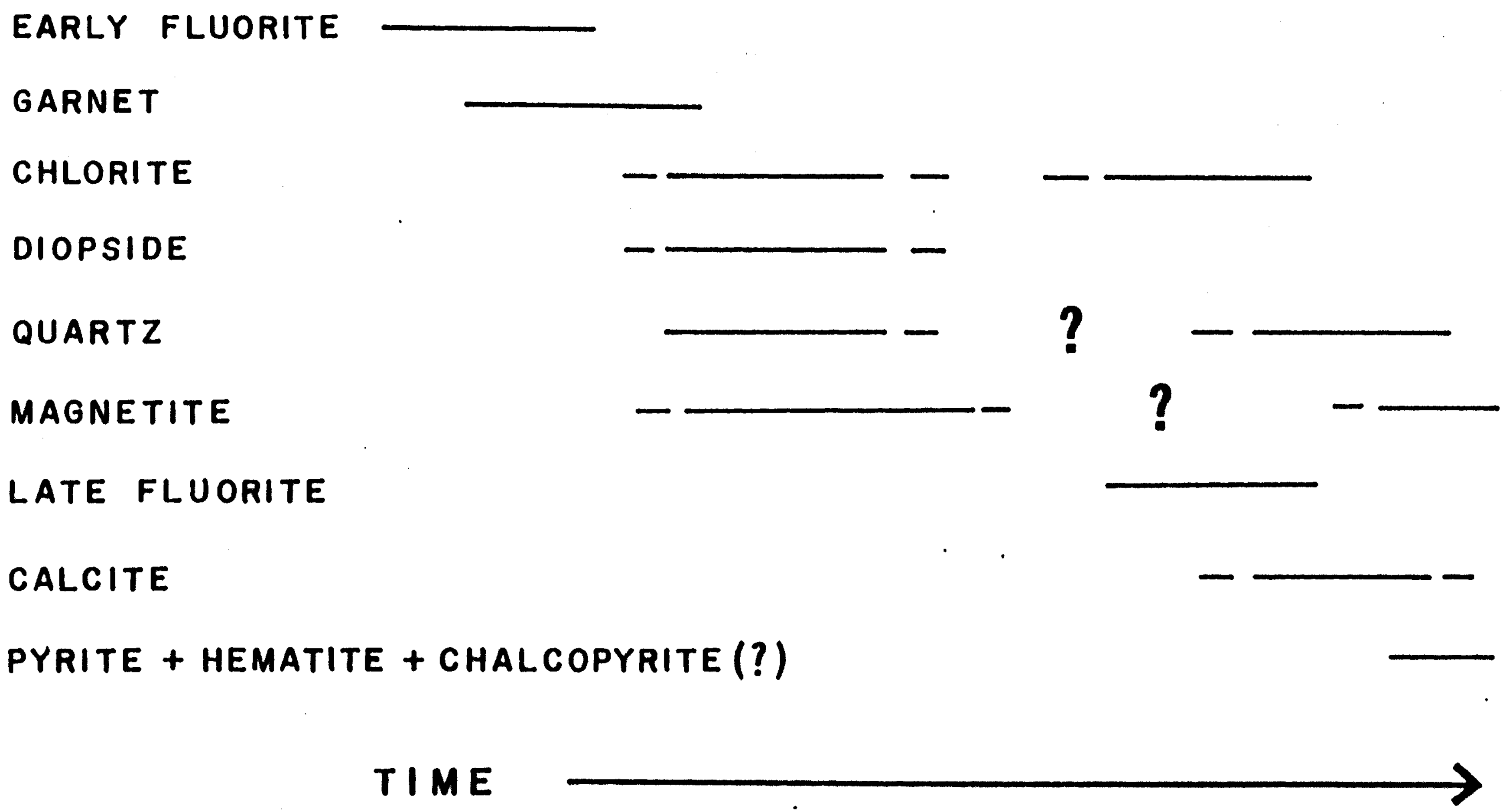

Figure 10. Paragenetic sequence of late hydrothermal minerals in skarn A.

clusters of cubic crystals deposited on late hexagonal quartz crystals. Early fluorite, constituting approximately 40% of the magnetite + fluorite skarn, is seen to vary in grain size between 0.6 and 3 mm, and is distinguished by its limonite-stained cleavages and its occurrence as replacements of (?) and open space fillings in earlier formed calc-silicates of the host rock. Late fluorite crystals are 1 to 3 mm in diameter, notably lack iron staining along cleavages, and occur as open space fillings.

Early fluorite displays interesting textural relationships with magnetite and the host rock minerals which are shown in the negative photomicrograph in Figure 11. Irregular rings of silica (?) around 'islands' of the fractured host rock appear to have formed as reaction rims (Location U, Figure 11). These silica (?) rings often form a boundary within which no fluorite is deposited (Location V, Figure 11). In other places in the photomicrograph (Location W, Figure 11), the reaction rims (?) served to confine areas of fluorite deposition. Still, in other instances, fluorite appears to have been deposited around nuclei of the fractured host rock (Locations X1 and X2, Figure 11). Therefore, the textural relationships are interpreted to indicate the deposition of fluorite in open spaces formed by the dissolution of the host rock calc-silicates.

Figure 11. Negative photomicrograph showing textural relationships in the magnetite + fluorite skarn body. -- White, black, and grey areas are, respectively, magnetite, fluorite, and relict host rock calc-silicates. Letters refer to examples of textures described in text.

Magnetite. Magnetite, comprising 50 to 60% of the magnetite + fluorite body, appears macroscopically as contorted laminae ≤ 3 mm in thickness continuous for a distance of 10 meters. Microscopically, magnetite occurs as botryoidal masses and as vermicular-like growths adjacent to the massive variety. The botryoidal masses occur as discrete elongate bodies, ≤ 5 mm long and 0.3 mm wide, with mushroom shaped extensions that, when formed side by side, give the rock a banded texture. Magnetite appears to have been deposited within and parallel to the silica (?) rings discussed earlier (Location Y, Figure 11), and as in the fluorite, magnetite was deposited around nuclei of the host rock. These textures suggest that magnetite, along with the fluorite, was deposited in open spaces in the original host rock. Vermicular magnetite is a distinct component of most magnetite bands (Location Z, Figure 11), occurring invariably on only one side of a single band, and on the same side of multiple bands. The worm-like replacements are ≤ 0.5 mm long by 0.1 mm wide that merge at one end into the massive magnetite, and that are often bounded at the other end by a microveinlet of limonite plus chlorite. This geometry is noted for its distinctive textural polarity which can be interpreted to reflect a deposition front.

Chlorite. Chlorite occurs as minor alteration after garnet and diopside in the garnet body and more abundantly with magnetite in the magnetite + fluorite body. In all occurrences, chlorite is euhedral tabular, pale to dark green, and $\leq$ 1 mm in diameter. Most chlorite has been replaced by magnetite and is, thus, earlier than magnetite. In addition, chlorite occurs along microfractures in early fluorite and as perpendicular growths to quartz (?) vein walls. However, some chlorite appears to form as a reaction rim around botryoidal masses of magnetite. A second phyllosilicate which was distinguished optically from the chlorite by its higher birefringence (lower 3rd order) occurs in close association with some chlorite and is tentatively identified as phlogopite or biotite.

Late Stage Minerals. Alteration is most discernible in the garnet because alteration appears to have occurred during deposition of magnetite. Alteration of garnet to diopside, chlorite, magnetite, and pyrite is common, and these alteration minerals compose up to 10% of the garnet skarn. Diopside is typically confined to the cores of the garnet crystals while only a few grains occur in quartz; a similar feature has been noted by Perry (1964). Chlorite replaces diopside, and magnetite occurs along microfractures and as discrete skeletal grains in garnet and diopside. Garnet and diopside are also replaced by an unidentified, radiating to crisscrossing acicular mineral that is light brown in plane light, but is too fine grained to determine its opitcal properties. The habit and host chemistry suggest that the mineral may be an amphibole.

In one prospect pit, a distinct assemblage of late minerals includes massive clear quartz ($\leq$ 70%) and clear quartz crystals (25%), cubes of fluorite (4%), and brown calcite, goethite, pyrolusite, chlorite, and magnetite totaling about 1%. The cubic fluorite is the same as the previously discussed late stage fluorite. The replacement of late calcite by magnetite indicates that magnetite was deposited also during the final stages of mineralization and alteration.

Fracturing of the Skarn

At least two periods of fracturing can be demonstrated to have occurred in the magnetite + fluorite skarn body. The earliest fracturing occurred in the calc-silicate 'islands' of the magnetite + fluorite skarn (~ 10-20 fractures/mm, Location U, Figure 11). The second period of fracturing is developed in the fluorite where disseminated chlorite and iron oxide coatings occur along cleavages, and is also manifest in the magnetite as veinlets of orange to brown iron oxide plus chlorite. In the garnet body adjacent to the magnetite + fluorite, only one period of fracturing can be clearly documented in thin section. Intense fracturing is represented by veinlets of limonite plus calcite plus or minus magnetite. Therefore, skarn A was probably localized by repeated fracturing. That intense fracturing has occurred in the vicinity of the skarn is supported by the observation that the only occurrence of strongly fractured Cochise Peak Quartz Monzonite (the hydrothermally altered quartz monzonite) is near skarn A.

Skarn B

Skarn B occurs in a small prospect along a N 40 E trending low angle fault that dips 20° to the northwest (Location B, Figure 7). The fault is parallel to and 6 meters west of the major fault between Cochise Peak Quartz Monzonite and Paleozoic rocks (Line AD, Figure 5). The skarn was studied because it contains a simple mineralogy whose formation can be attributed to rehydration of hornfelsed Abrigo limestone along a fault. At skarn B, the Abrigo Formation is approximately 7 meters thick and can be divided into three distinct units: 1) a lower 3 meter thick siliceous unit, 2) a middle 2 meter thick calcareous member and 3) an upper 2 meter thick siliceous unit. The two siliceous units are strongly brecciated, a feature which is seen best on the weathered surface where clasts and matrix weather to different shades of brown. On a fresh surface, the siliceous hornfels is a dense, black or blue rock that contains disseminated pyrite and pyrrhotite, and shows transported iron oxide films.

The calcareous unit consists of garnet, composing up to 60% of the rock, clinozoisite (20%), diopside (10%), and vesuvianite (10%). The garnet is pale green and is confined to bedding planes, suggesting that it was formed by isochemical metamorphism of siliceous interbeds in the calcareous Abrigo. In thin section, garnet is isotropic except in a few areas where anisotropy is evidenced by zoning of alternating interference colors. In plane reflected and transmitted light, garnet is seen to be strongly pitted, and grain boundaries are lined with a pale brown iron oxide or clay mineral. The composition of the garnet is probably toward the grossular end member in the ugrandite solid solution series as suggested by its color and its occurrence within silty interbeds of Abrigo limestone. As the fault is approached in the calcareous bed, vesuvianite, calcite, muscovite, and diopside, which is more euhedral and coarser grained than the diopside that replaces garnet, increase in amount until they compose the entire rock. The deposition of this assemblage of minerals, beginning with the precipitation of diopside, marks the initiation of weak Mg^{++} metasomatism and rehydration of earlier formed contact metamorphic minerals.

Description of Minerals Near the Fault

Diopside and Sanidine. Diopside, composing up to 80% of the skarn, occurs as pale green, medium to coarse grained euhedral crystals, $\leq$ 5 mm wide and 1 cm long, with perfect (110) cleavage. In thin section, subhedral to euhedral crystals with a crystalloblastic texture show multiple and paired twinning on (100). Typically, diopside has a pitted to shattered appearance caused by crackle-like fracturing and alteration along cleavage planes. Randomly oriented hairline fractures (~ 4 fractures/mm) are frequently stained with a brown oxide mineral. A dark brown manganese oxide, making up < 1% of the rock, occurs around grains of altered diopside. The presence of Mn in diopside was confirmed by microprobe analysis (Sample 66, Appendix A).

A few relict crystals of low sanidine were distinguished from orthoclase by their low 2V angles (10-20°), and were further identified by oscillitory zoning, crystal habit, and twinning. Sanidine is partially replaced by diopside, vesuvianite, and calcite. Diopside and sanidine were the earliest formed minerals, with sanidine formation overlapping later diopside and vesuvianite deposition. The more common replacement of diopside by vesuvianite and the euhedral intergrowths of the two suggest that vesuvianite formed during late stages of diopside deposition.

<u>Vesuvianite</u>. Vesuvianite, composing ~ 15% of the skarn, occurs as long, ≤ 6 mm to 3 cm, dark green, slightly radiating prismatic clusters. In thin section, vesuvianite is seen to be characterized by zoning of anomalous green interference colors and moderate (110) cleavage development parallel to the prisms. Alteration is particularly noticable in the cores where fracturing and replacement by calcite along cleavage planes is best developed. Common fracturing, perpendicular to cleavage, forms an interlocking network of fractures typically filled with calcite that enhances the shattered appearance of most vesuvianite crystals. Although vesuvianite prisms often appear to grow into calcite, they more commonly share euhedral grain boundaries with calcite, or are replaced by calcite indicating that vesuvianite is probably slightly older than calcite. One microprobe analysis of vesuvianite is given in Appendix A (Sample 67).

<u>Calcite and Muscovite</u>. Calcite and muscovite appear as late minerals replacing diopside and vesuvianite. Calcite, composing between 5 and 10% of the skarn, occurs in interstitial sites within the diopside. In addition, calcite occurs as veinlets and impregnations along cleavages of diopside and vesuvianite. Minor alteration of calcite is evidenced by fading of birefringent colors. Muscovite occurs in fine grained (≤ 0.5 mm) masses and as coarse grained (~ 2-3 mm) aggregates that appear to be grossly

vein controlled. In thin section, tabular muscovite aggregates display classic birds-eye extinction. Minor replacement by calcite does not marr the fresh appearance of most grains.

Other Skarn Deposits

Several other skarn deposits within the study area are shown in Figure 7. These skarns are localized by faults and, like skarns A and B, appear to have formed by metasomatic processes. By far, the most abundant mineral in these skarns is garnet, constituting up to 95% of the rock in some skarns. The garnet is typically light brown, well zoned, and weathers out as small crystals. The minerals magnetite, hematite, chalcopyrite, malachite, and azurite are common associates of garnet. A few of the more distinct skarns mentioned below are located in Figure 7.

Skarn C is noted for its size and texture. Massive brown garnet containing stringers of iron oxide aligned in the direction of the fault forms a band 75 meters long by 15 meters wide along a drainage. Skarn D is noted for the occurrence of large, 4 cm long, radiating masses of epidote or clinozoisite crystals. A third skarn (Location E, Figure 7) warrants a brief description because of its distinct mineralogy and because from it a small amount of zinc production was won. Skarn C contains stringers and pods of pyrite and brown to black sphalerite with lesser amounts of galena, pyrrhotite, and chalcopyrite. These sulfides replace silicated marble of the Upper Paleozoic rocks along a N 80 W trending fault that dips 26^{o} to the northeast. The host rock is a pure marble which is locally silicified or replaced by green garnet. The sulfides replace both calcite and garnet and occur with other dark green minerals (hardnesses > 5.5) that are probably calc-silicates, but whose exact identity could not be determined macroscopically. Sulfide paragenesis was determined from four polished sections to be early pyrite replaced by pyrrhotite. Sphalerite with exsolved chalcopyrite and discrete grains of chalocopyrite are cogenetic or slightly later than pyrrhotite, and galena was deposited last. The limited amount of sulfide replacement and lack of extensive alteration in all of the above skarns, indicates that mineralization is weakly developed in the study area.

Petrographic study of minerals in skarns A and B helped to establish mineral paragenesis, but often these textural studies are not definitive. Another way to investigate the sequence of mineral deposition is by examining the thermal history of several minerals if the overall thermal environment is known. The thermal evolution of the skarns in this study was documented by fluid inclusion studies.

FLUID INCLUSION STUDIES

Fluid inclusions in various skarn minerals were studied to determine temperature, salinity, and pressure attending skarn formation. Inclusions were heated and cooled in a dual-purpose heating-freezing stage, using the methods described by Roedder (1962, 1963, 1967). Temperatures were measured with a chromel-alumel thermocouple attached to a digital readout meter. To insure reproducibility within $\pm$ 2°C for homogenization runs and $\pm$ 0.5°C for freezing determinations, inclusions were heated and frozen at least twice. In order to simplify the discussion of fluid inclusion data, the temperatures, pressures, and salinities determined from individual minerals are presented separately.

Skarn A

Fluid inclusions were studied in garnet, quartz, and fluorite to document changing characteristics of the mineralizing fluids during skarn formation. Homogenization temperatures for these minerals are plotted in histogram form in Figure 12.

Garnet

Primary fluid inclusions in garnet, varying in size between 2 and 10 microns, occur principally in grain cores and are composed of two phases, liquid and vapor. Some primary inclusions occur along distinct overgrowth zones while other more abundant secondary or psuedosecondary inclusions, too small to study, line microfractures. None of the inclusions in garnet contain daughter minerals. Inclusions in garnet homogenize between 300° and 460°C with the majority of temperatures between 360° and 440°C and maxima at 420°-440°C. A few vapor-rich and liquid-rich inclusions, also principally in the garnet cores, had not homogenized by 530°C, suggesting deposition of garnet at higher temperatures from boiling solutions.

The suggestion that boiling solutions were present during garnet formation provides information on corresponding salinities and pressures. Salinities of the fluids could not be determined by the freezing point depression method (Roedder, 1963) because the fluid inclusions did not freeze even when temperatures were supercooled to -120°C. However, a maximum salinity of 26.4 weight percent NaCl, the saturation value of an aqueous NaCl solution at 25°C, is indicated by the absence of halite as a separate phase at room temperature in the inclusions. A minimum value of approximately 14 weight percent NaCl is required to expand the critical point in the system H_2O - NaCl to 530°C (Sourirajan and Kennedy, 1962). A solution containing 14 weight percent NaCl equivalent provides a minimum salinity for fluids because no supercritical phenomena were observed at 530°C. Supercritical behavior is characterized by the fading, rather than the expansion or contraction, of the meniscus. Although the filling temperatures and salinities of these high temperature inclusions are not exactly known, a minimum temperature of 530°C and maximum salinity of approximately 26.5 weight percent NaCl indicate a corresponding minimum pressure of approximately 680 bars. The lower temperature garnet, deposited around 400°C, indicates a minimum pressure of 220 bars for a 25 weight percent NaCl equivalent solution. These relationships are represented in Figure 13 which shows the two phase boundary for various NaCl salinities in the system H_2O - NaCl. Furthermore, a maximum pressure of ~ 1250 bars is defined by the intersection of the H_2O - NaCl critical curve with the Orthoclase - Albite - Quartz melting curve (Holland, 1967). Using the minimum values of pressure, the amount of overburden during mineralization is calculated for both hydrostatic and lithostatic loads from the equation:

$$P_{bars} = \rho g h,$$

where P is the pressure in bars, ρ is the density of water or rock, g is the acceleration due to gravity and h is the height, in meters, of the column of water or rock over the skarn. For a minimum pressure of 680 bars, the hydrostatic load, assuming a density of 0.8 gm/cc (Urusova, 1975), corresponds to a depth of 8700 meters, whereas the lithostatic load, using a density of 2.85 gm/cc is 2400 meters. Likewise, for a minimum pressure of 220 bars, the amount of overburden assuming a hydrostatic and lithostatic load is, respectively, 2800 and 800 meters.

Quartz

Fluid inclusions in quartz are present in the milky variety that occurs interstially to, and as crosscutting veins in, the garnet. The inclusions vary between 2 and 50 microns in diameter. Fracturing which is responsible for leaking and necking down were present in at least 60% of the inclusions, and thus, only fluid inclusions that were equidimensional and without irregularities were used. If inclusions subjected to either of these phenomena had been measured, homogenization temperatures would have been greater or less than their real values. Fluid inclusions in quartz are composed of two phases, and include both liquid-rich and vapor-rich types; no daughter minerals were observed. Homogenization temperatures of fluid inclusions in quartz are between 200° and 400°C with a majority between 300° and 380°C and a maximum at 360°-380°C (Figure 12). Fluid inclusions homogenized to a liquid phase or a vapor phase within the range 340°-400°C indicating that quartz was precipitated from boiling solutions. Because the fluids were on the H_2O two phase boundary, no pressure correction is needed for the homogenization temperature, and the approximate range of

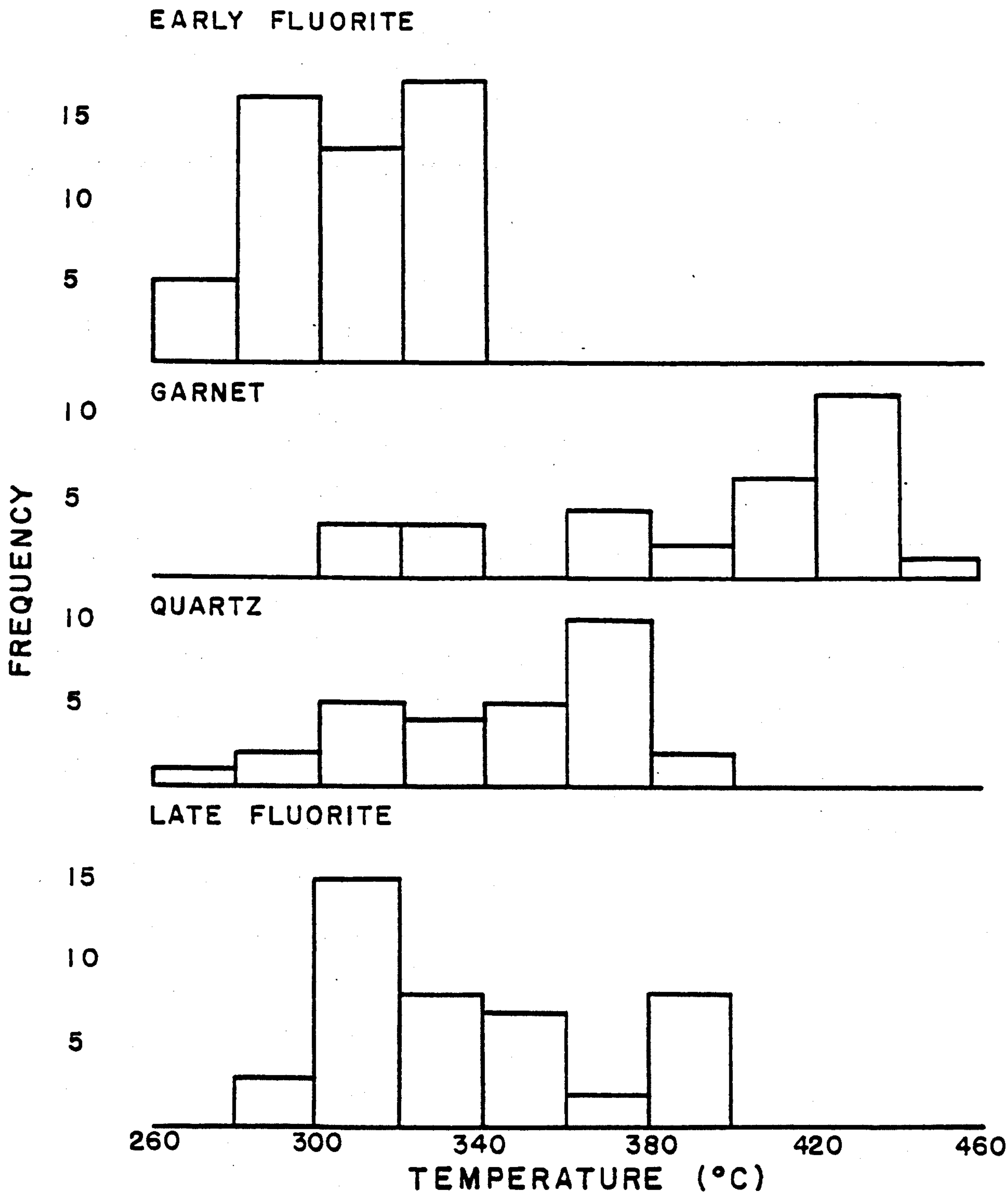

Figure 12. Histogram showing homogenization temperatures of fluid inclusions in minerals in skarn A.

pressures can be read from the boiling curve of appropriate NaCl equivalent salinity (Figure 13).

Salinities could not be determined by the freezing point depression method because, as in the garnet, inclusions in quartz would not freeze. However, since no critical behavior was observed during homogenization, the critical point in the system H_2O - NaCl must be expanded to at least 400°C which corresponds to a minimum salinity of 2.6 weight percent NaCl equivalent (Sourirajan and Kennedy, 1962). A maximum salinity of 26.4 weight percent is the saturation value of an aqueous NaCl solution at 25°C. These salinities indicate a total pressure between 115 and 280 bars during quartz deposition (Figure 13). If hydrostatic pressure is assumed, the maximum height of a column of water is obtained from boiling data given by Haas (1971) to be 2500 meters and 4300 meters for a 25 and 2 weight percent NaCl equivalent solution, respectively (Figure 14). If lithostatic pressure is assumed, the maximum amount of overburden is calculated with a density of 2.85 gms/cc to be approximately 1000 meters.

In addition to total pressure, maximum f_{CO_2} can be determined from miscibility data in the system CO_2 - H_2O. No separate CO_2 phase was observed in the inclusions at room temperature which is below the critical temperature (31.1°C) of CO_2. Therefore, the maximum amount of CO_2 in the inclusions is that considered by Nash (1976; 3 mole percent) and

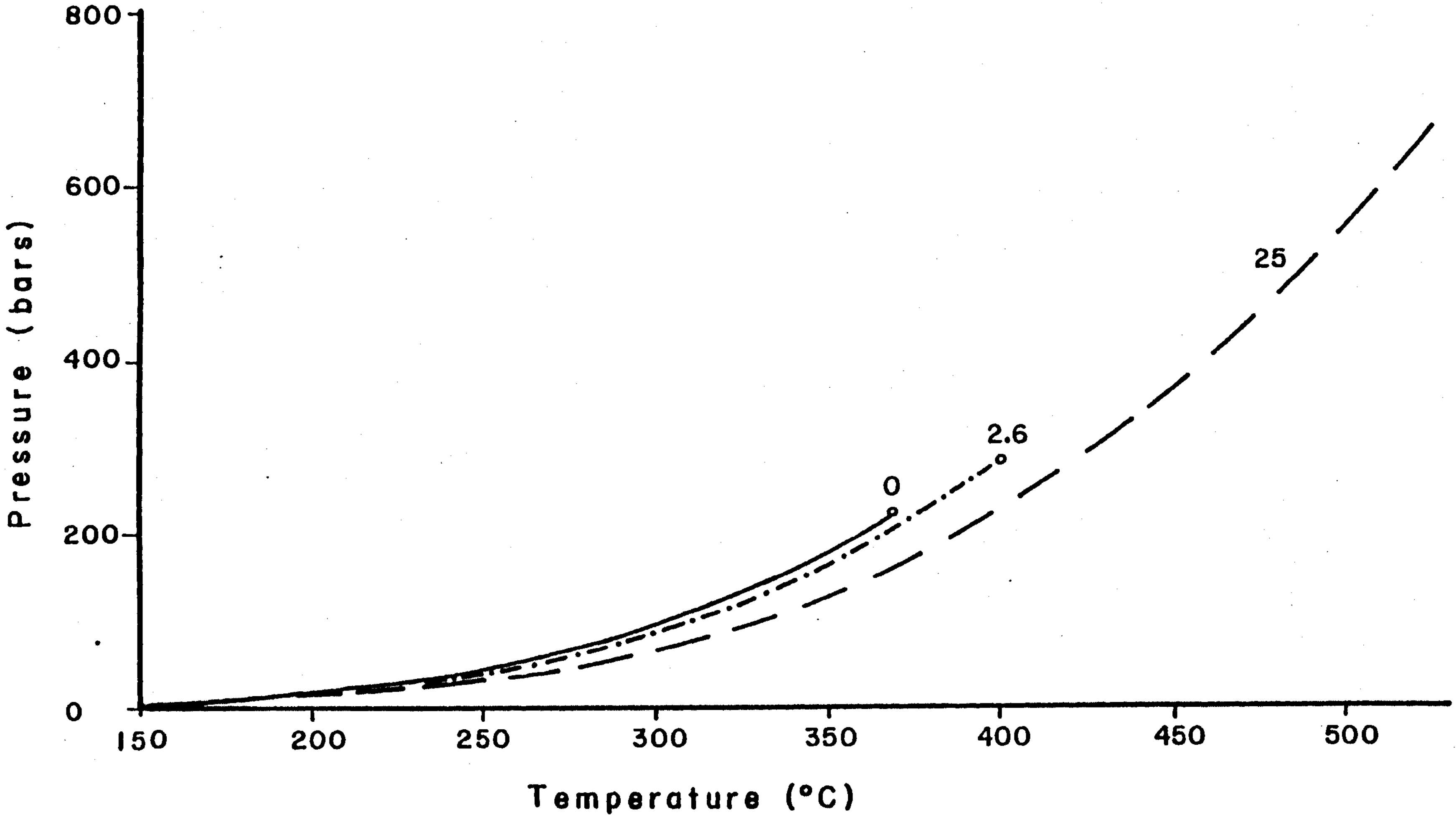

Figure 13. Phase diagram for the system H_2O - NaCl. -- Numbers on graph are weight percent NaCl in solution with corresponding critical points as open circles. Data from Haas (1971) and Sourirajan and Kennedy (1962).

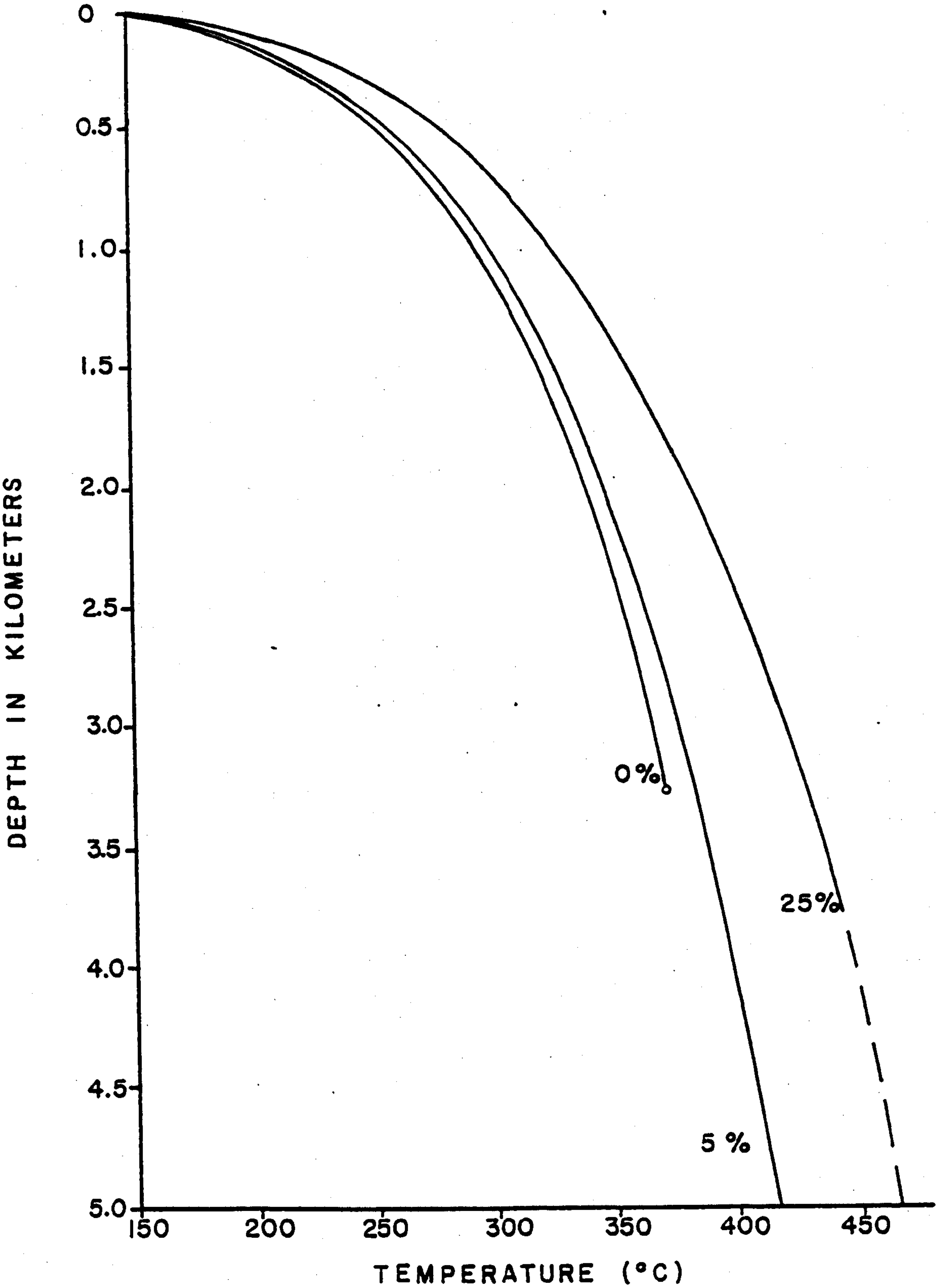

Figure 14. Two phase boundaries of pure water and aqueous NaCl solutions containing 5 and 25 weight percent NaCl. -- Data from Haas (1971).

Kerrick (1977; 10 mole percent) to be the lower limits of a detectable CO_2 phase. With this limitation, the maximum f_{CO_2} can be calculated from the expression:

$$K = \frac{f_{CO_2}}{x_{CO_2}},$$

where K is Henry's Law coefficient for the solution of carbon dioxide in aqueous NaCl solutions and x_{CO_2} is the mole fraction of CO_2. K values, given by Ellis and Golding (1963), were used at 25°C instead of 400°C because the lower value represents the temperature at which the inclusions were observed and it gives the least restrictive values of f_{CO_2}. Thus, for a 0.5 molal (3 weight percent) NaCl solution, at 25°C, K equals 1800 resulting in maximum f_{CO_2} values for a 10 and 3 mole percent CO_2 solution of 180 and 54 bars, respectively. In higher salinity solutions, the solubility of CO_2 is depressed, and for a 20 weight percent aqueous NaCl solution, the mole percent of CO_2 in solution drops to zero (Takenouchi and Kennedy, 1965). Therefore, the upper limit of f_{CO_2} was approximately 180 bars during quartz formation.

Fluorite

Fluid inclusions in fluorite indicate that fluorite was precipitated from two distinct fluids, referred to as early and late. Early fluorite contains inclusions that average between 10 and 20 microns in diameter and that typically contain four or five phases: vapor, liquid, halite, magnetite, and often sylvite. Halite and sylvite were identified by criteria discussed by Nash (1976) while magnetite was identified by its habit, color, and movement in a magnetic field. The homogenization behavior of these inclusions is similar to that described by Bodnar (1978); the inclusions homogenize to the liquid phase at temperatures lower than the temperatures for the dissolution of halite indicating that the better estimate of trapping temperatures is that of salt dissolution which occurs between 260^{o} and 340^{o}C. Using these temperatures and the phase diagram for the system H_2O - NaCl - KCl (Roedder, 1971, p. 114), gross estimates of salt concentrations can be determined. Inclusions with NaCl daughter minerals indicate an average salinity of 37 weight percent (10 molal) NaCl while inclusions containing both NaCl and KCl daughter minerals indicate respective salinities of 32 weight percent (10 molal) and 14 weight percent (2.2 molal). Dissolution temperatures of both KCl and NaCl from 8 inclusions in addition to their corresponding salinities are shown in Table 1. These data can be used to calculate a K/Na ratio for the solutions from which early fluorite was deposited. K/Na molar ratios are listed adjacent to the weight percents of KCl, NaCl, and NaCl equivalent for each of the 8 inclusions, and give an

Table 1. Dissolution Temperatures of NCl and NaCl in 8 Inclusions with Corresponding Weight % Approximated from the Phase Diagram for the System H_2O - NaCl - KCl of Roedder (1971, p. 114).

INCLUSION	TEMPERATURE (°C) OF DISSOLUTION		WEIGHT % SALTS			MOLAR
	KCl	NaCl	KCl	NaCl	NaCl Equiv.	K/Na
1	81.7	264.7	17.1	26.2	36.3	0.28
2	78.9	308.5	16.3	29.7	39.3	0.26
3	65.9	302.7	14.0	30.8	39.0	0.22
4	69.0	333.4	14.5	31.5	40.0	0.23
5	69.5	334.0	14.6	31.8	40.4	0.23
6	64.3	326.4	14.1	31.8	40.1	0.22
7	65.0	334.0	13.9	32.3	40.5	0.22
8	65.8	334.0	14.3	32.2	40.6	0.22

average K/Na ratio of 0.23. The NaCl and KCl weight percent values are, at best, approximations of the salinities because 1) Roedder's graph is based on a three component system, whereas the fluid inclusions in this study usually contain a fourth known component, Fe_2O_3, and probably additional unknown components in solution, and 2) Roedder's graph was calculated from data from the two phase boundary, and the temperature of total homogenization is that of the disappearance of an H_2O vapor phase. In this study, the dissolution of NaCl postdates the disappearance of the vapor bubble, and therefore, the solution was above the two phase boundary during trapping. Because no data exist for the effects of pressure and temperature on saline solutions off the two phase boundary, Roedder's data is used to approximate the salinites.

An approximate minimum pressure attending early fluorite déposition can be determined from the data of Urusova (1975). At 350°C and for a 40.1 weight percent NaCl boiling solution, the pressure is 110 bars. Because no boiling was observed in the fluorite inclusions, this pressure provides a minimum value. Assuming a hydrostatic head with a density of approximately 1.06 gms/cc, the depth to mineralization is 1100 meters. Assuming a lithostatic load with a density of 2.85 gms/cc, the depth to mineralization is 400 meters.

Late fluorite has inclusions that average between 10 and 20 microns in diameter and contain two or three phases, namely, liquid, vapor, and a daughter mineral of undetermined composition. The unidentified daughter mineral has a columnar habit, square cross section, moderate birefringence, and symmetrical to parallel extinction. All inclusions homogenized to the liquid phase between 300° and $400^{\circ}C$, but the daughter mineral never dissolved. Because these inclusions do not have halite daughter minerals, salinities could not be estimated from homogenization temperatures; instead, salinities were determined using the freezing point depression method described by Roedder (1963). The range of freezing points for 22 inclusions is -1.0 to $-2.0^{\circ}C$. The average freezing point is $-1.21^{\circ}C$ which corresponds to a solution containing 1.8 weight percent (0.3 molal) NaCl equivalent. As seen from the graph in Figure 13, a minimum pressure of approximately 100 bars accompanied late fluorite deposition. Using these data, the pressure correction for homogenization temperatures are estimated from the graphs of Potter (1977) to be $\leq 10^{\circ}C$.

Skarn B

Diopside was the only mineral from skarn B that contained fluid inclusions conducive to study. The inclusions, which are approximately 40 microns in diameter, contain liquid, vapor, and halite that homogenize to the liquid phase in the range 480°-550°C. The salinity of the solutions was determined by referring the halite dissolution temperatures (380°-445°C) to the NaCl solubility graphs of Potter, Babcock, and Brown (1977), which give values in the range 44 to 50 weight percent NaCl equivalent. In all homogenization runs, the temperature of salt dissolution was lower than the temperature at which the vapor bubble disappeared. This relationship is displayed on the graph in Figure 15 which shows that for each inclusion the filling temperature is always greater than the temperature of salt dissolution (i.e., all points lie above the 1:1 line). The widespread distribution of points indicate that the salinities fluctuated during the deposition of diopside. A minimum pressure can be approximated by referring the maximum homogenization temperatures (~ 550°C) and salinities (~ 50 weight percent NaCl equivalent) to the charts of Urusova (1975). For a boiling solution with these characteristics, the corresponding pressure is 570 bars. The corresponding depths to skarn formation are 5800 meters and 2000 meters, respectively, for a hydrostatic load with a density of 1.0 gm/cc and a lithostatic load with a density of 2.85 gms/cc.

The temperatures, pressures and salinities that existed during the formation of both skarns A and B can be used in conjuction with mineral parageneses to document the environment of skarn formation.

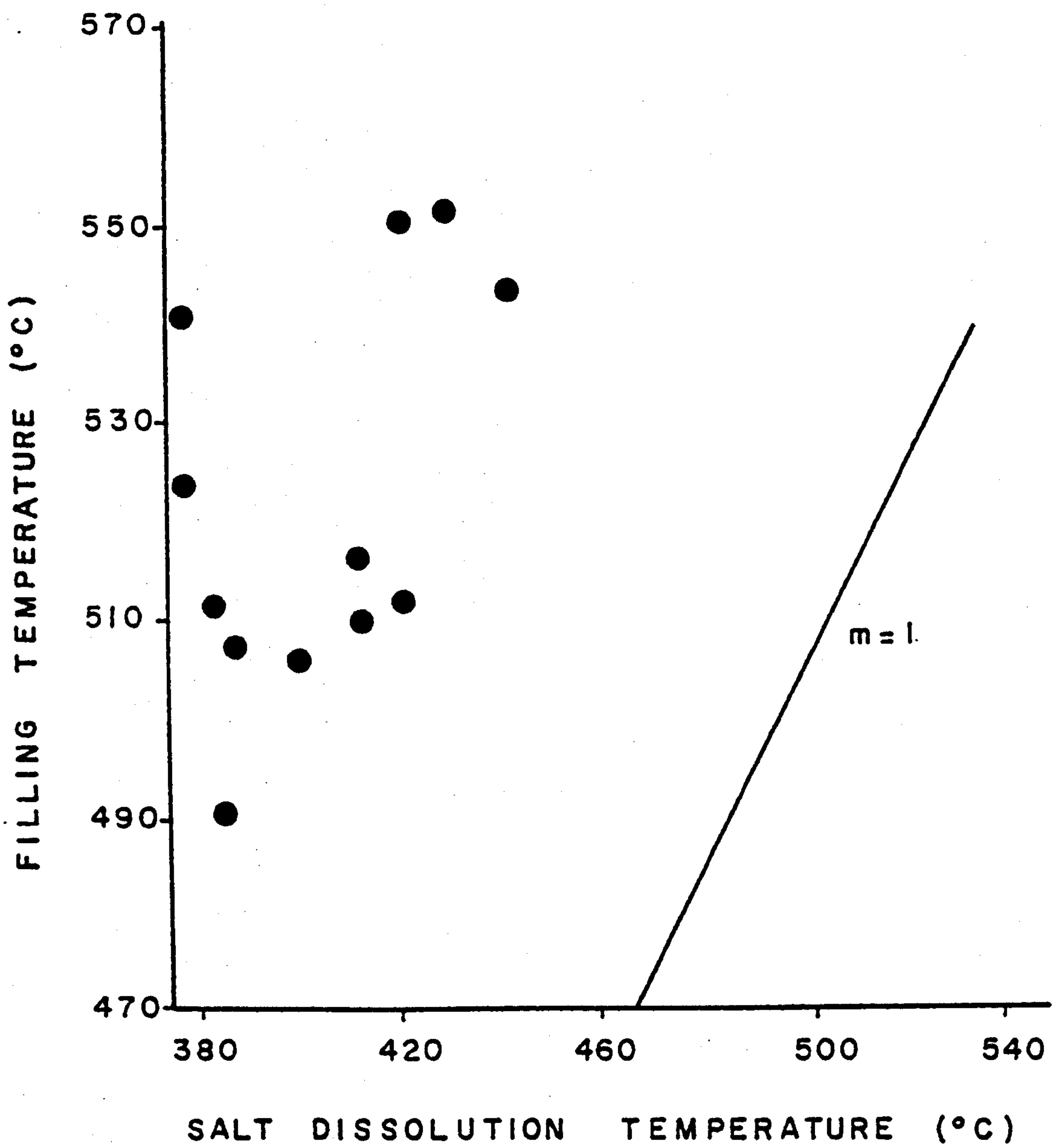

Figure 15. Graph showing filling temperatures vs. salt dissolution temperatures for fluid inclusions in diopside. -- The occurrence of points above the line of slope 1 indicates that the filling temperature (i.e., the temperature of the disappearance of the vapor bubble) is invariably higher than the salt dissolution temperature.

ENVIRONMENT OF DEPOSITION

Skarn A

Mineral paragenesis and fluid inclusion studies suggest that skarn formation was initiated by the deposition of fluorite between 280° and 340°C from non-boiling saline solutions containing 37 to 46 weight percent NaCl + KCl. Temperatures increased to at least 530°C while salinities decreased to 14-26.4 weight percent NaCl equivalent during garnet deposition. Although some garnet was apparently deposited from boiling solutions at temperatures greater than 530°C, most of the garnet was precipitated from non-boiling solutions at lower temperatures between 360° and 440°C. After the initial rise, the temperatures decreased to the range 300° to 380°C during the deposition of quartz and remained stable through the precipitation of late fluorite. Therefore, with the exception of high temperature inclusions in garnet, temperatures were essentially within a broad constant range (250°-400°C) as depicted in Figure 16. Paragenetic relationships of alteration minerals indicate that diopside and chlorite were deposited through a period contemporaneous with quartz deposition (Figure 10). By the time late fluorite was being precipitated, the salinities had decreased to 1.8 weight percent NaCl equivalent, suggesting

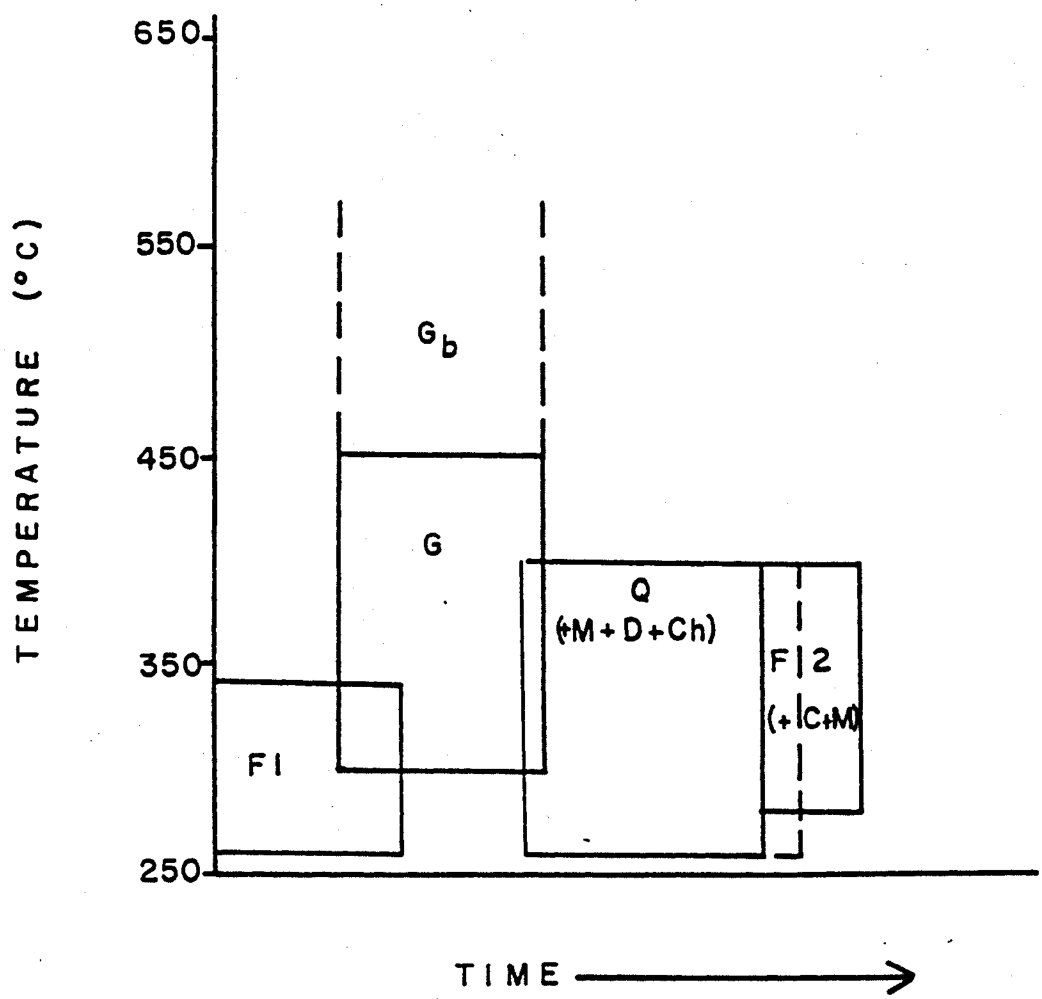

Figure 16. Graph showing the evolution of temperatures during the deposition of minerals in skarn A. -- F1, early fluorite; G, garnet; G_b, garnet deposited from boiling solution; Q, quartz; F2, late fluorite; M, magnetite; D, diopside; Ch, chlorite; C, calcite. Note that except for boiling during garnet deposition, temperatures were relatively constant.

that the original saline solutions were progressively diluted with low salinity water or that a new solution was introduced. Overlapping the deposition of late fluorite is that of late chlorite and calcite. The paragenetic positions of the metallic minerals magnetite, pyrite, hematite, and chalcopyrite are more difficult to discern. Magnetite replaces early but not late fluorite, indicating its deposition between the two, although minor magnetite replaces late calcite indicating precipitation of paragenetically late magnetite. The start of magnetite precipitation is thought to overlap chlorite deposition based on petrographic studies discussed earlier. Pyrite, minor hematite, and chalcopyrite occur with late magnetite as crosscutting veinlets and disseminations in late stage minerals such as calcite, quartz, and chlorite.

The minimum pressures attending formation of early fluorite, garnet, quartz and late fluorite, in addition to the maximum pressure attained during quartz deposition, are shown in a pressure - time plot in Figure 17. Because most of the indicated pressures in Figure 17 are minima, the only definitive break in pressure is seen to occur between garnet and quartz deposition where the pressure drops from a minimum of 680 to a maximum of 280 bars. The change in deposition of garnet from boiling solutions to deposition of quartz from non-boiling solutions marks this drop in pressure. Figure 18 shows the corresponding depths to mineral formation calculated

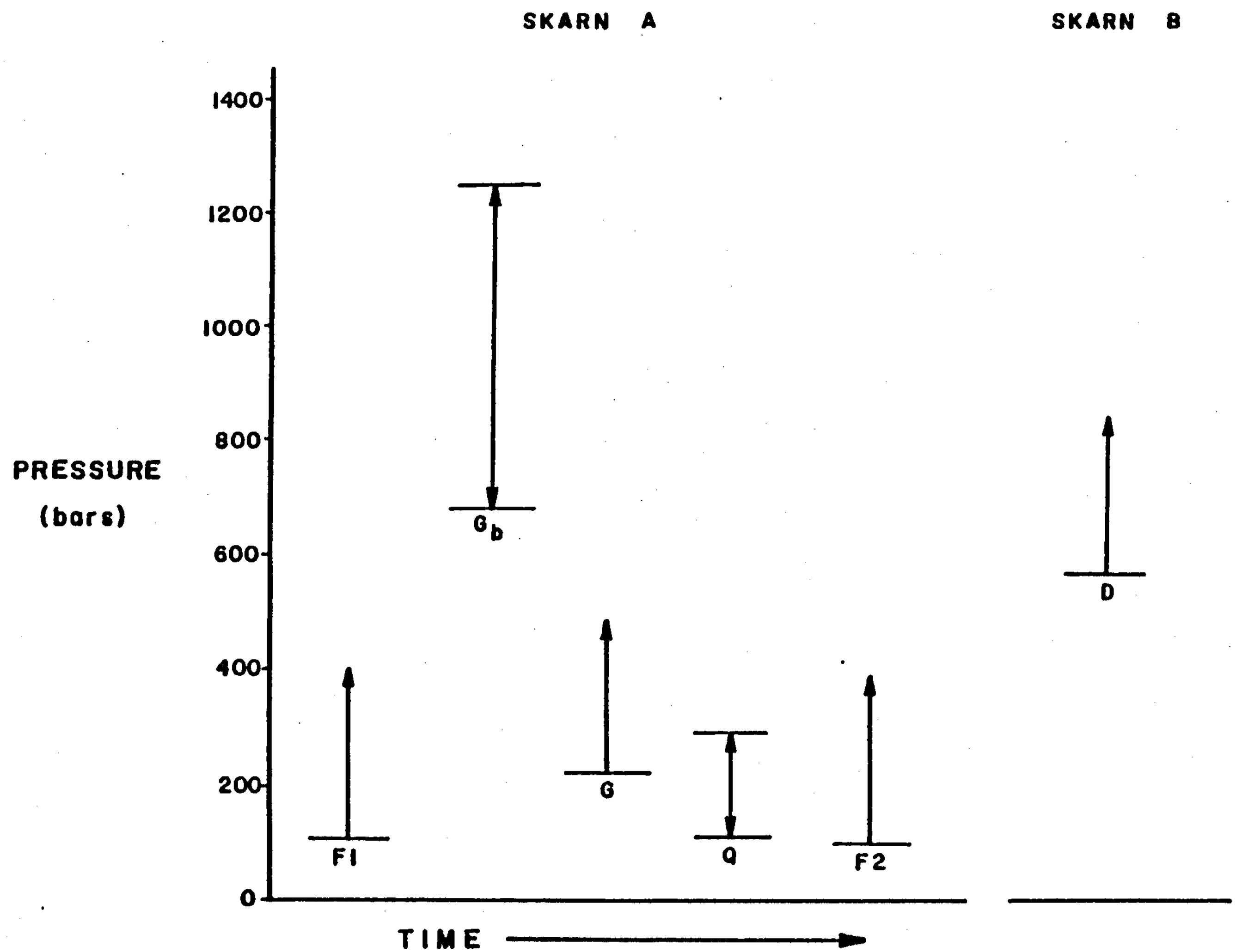

Figure 17. Graph showing pressures attending the formation of minerals in skarns A and B. -- F1, early fluorite; F2, late fluorite; G, garnet; G_b, garnet deposited from boiling solutions; D, diopside; Q, quartz. Only minimum pressures are given for F1, F2, G, and D.

for both hydrostatic (H) and lithostatic (L) loads. The lower depth limit for the formation of garnet (G_{b_L}) under a lithostatic load corresponds to the pressure at which the critical curve in the system H_2O - NaCl intersects the minimum melting curve in the system Orthoclase - Albite - Quartz. Q_{H1} and Q_{H2} were calculated, respectively, for the end member salinities 2.6 and 26.4 weight percent NaCl equivalent of the solutions depositing quartz. Because the Stronghold Granite, which surrounds skarn A, has the characteristics of an epizonal pluton (Gilluly, 1956), the depth of burial is probably less than the epizone - mesozone boundary of 6.4 km (Buddington, 1959). Therefore, the minimum depth value, assuming hydrostatic pressure, for the formation of garnet from boiling solutions (Line G_{b_H}, Figure 18) is probably invalid, and it is probable that the garnet showing homogenization temperatures greater than 530°C formed under lithostatic pressures. Also, it is unlikely that during skarn formation the minimum amount of overburden represented by the lines $F1_L$, G_{b_L}, G_L, Q_L, and $F2_L$ in Figure 18, changed by 1000 meters since there is no evidence for syn-mineralization faulting at skarn A. Thus, because the minimum overburden is greatest during garnet formation, assuming lithostatic pressure, the most general estimate of minimum depth during skarn formation is that defined by line G_{b_L} in Figure 18. Since the minimum depth of cover during skarn formation, represented by the

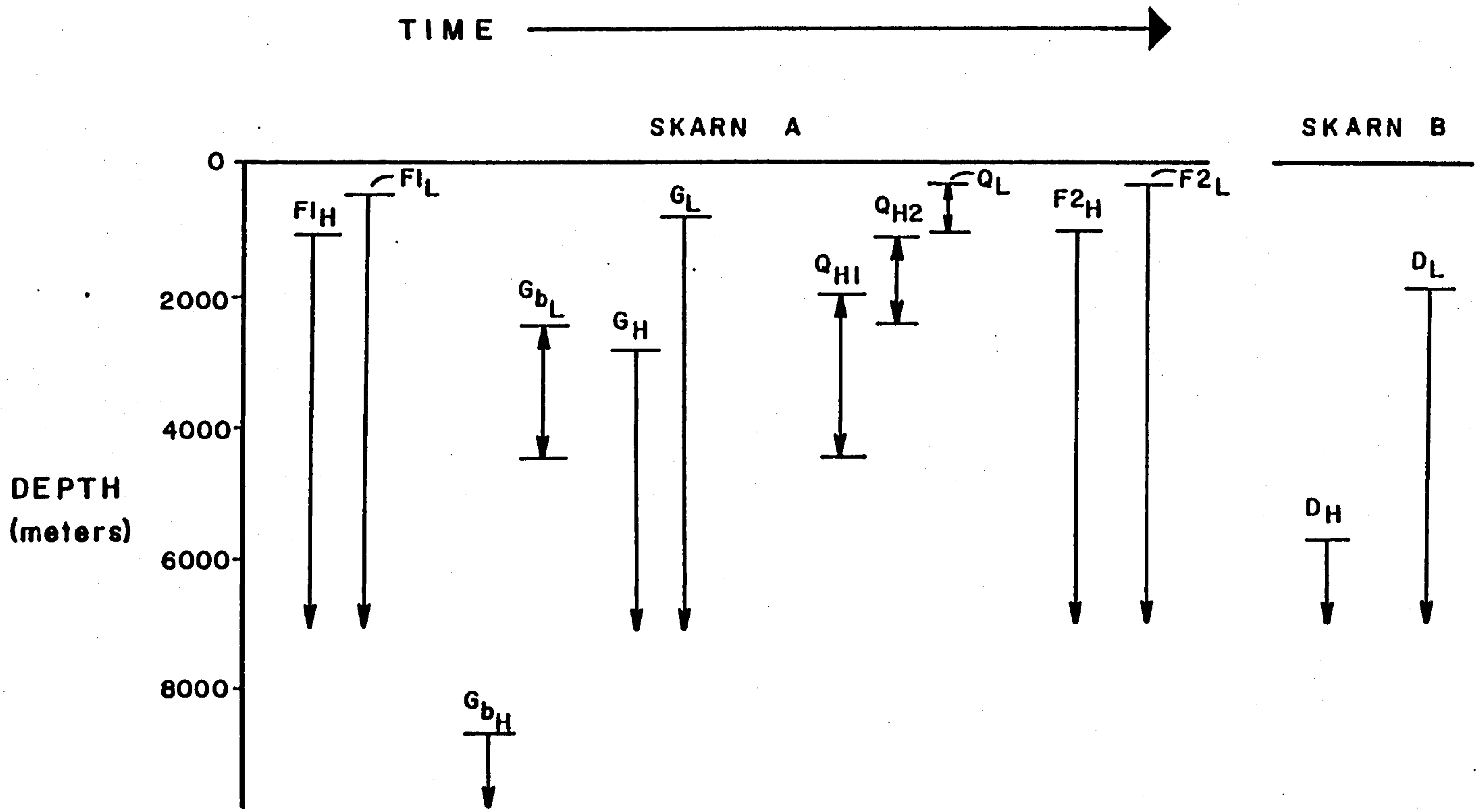

Figure 18. Graph showing minimum depths of burial during the formation of minerals in skarns A and B. -- H, hydrostatic pressure; L, lithostatic pressure. Letters are the same as those in Figure 17. Two depth intervals for Q_H refer to the two different solution salinities discussed in the text.

line Gb_L, is <u>assumed</u> to be 2300 meters, quartz must have been deposited under hydrostatic pressure from solutions containing approximately 2.6 weight percent NaCl equivalent. Furthermore, the minimum depth of formation under hydrostatic pressure of the lower temperature garnet (G_H) occurs in the depth range for the formation of quartz (Q_{H1}). Therefore, sometime during the deposition of garnet, or between the deposition of garnet and quartz, pressure appears to have dropped from 680 to 280 bars accompanied by a change from lithostatic to hydrostatic pressure. This change in pressure has been documented only at this locality and could be a local phenomenon.

Mineral Stabilities

Stability relationships of minerals in skarn A are used to document the evolution of skarn formation, and because mineral stabilities are dependent on temperature, they provide a check of the fluid inclusion geothermometry presented earlier. The phases used in the calculation (garnet, magnetite, quartz, pyroxene, and calcite) are represented by the components CaO, SiO_2, MgO, Al_2O_3, Fe, O_2, and CO_2. Al_2O_3 can be eliminated from consideration if garnet is written as the andradite component with non-unit activity, and likewise, MgO can be eliminated if pyroxene is written as the hedenbergite component with non-unit activity. The activities of these solid solution components may be calculated assuming

$a_i = N_{Fe}^j$ (Helgeson and others, in press) where N = mole fraction of the andradite and hedenbergite component of garnet and pyroxene, respectively, and j = the number of equivalent sites for Fe in each mineral (2 for garnet, 1 for pyroxene). Also, the chemical potential of SiO_2 is fixed by the presence of quartz.

Using the above boundary conditions, reactions can be written that represent the observed mineral paragenesis in skarn A. Omitting the minerals of skarn A not defined by this system, the mineral paragenesis is: early garnet followed by pyroxene plus magnetite, quartz, and calcite. In addition, calcite occurs as an early ubiquitous mineral in the host rock (Figure 9) which suggests it represents a saturation phase during skarn formation. The reactions:

1) $3CaCO_3 + 3SiO_2 + 2Fe^{+++}_{aq} + \frac{3}{2}O_2 = Ca_3Fe_2Si_3O_{12} + 3CO_2$

2) $CaCO_3 + 2SiO_2 + Fe^{++}_{aq} + \frac{1}{2}O_2 = CaFeSi_2O_6 + CO_2$ and

3) $2Ca_3Fe_2Si_3O_{12} + 5CO_2 = CaFeSi_2O_6 + Fe_3O_4 +$

$CaCO_3 + 4SiO_2 + \frac{1}{2}O_2$

describe mineral sequences observed petrographically. Sequence (1) is documented by the conversion of the host rock to andradite garnet. Sequence (2) is documented by pyroxene stability, and sequence (3) is suggested by the contemporaneous deposition of pyroxene and magnetite that postdates garnet deposition. Equilibrium boundaries for the above reactions are shown in Figure 19 in terms of the variables: log f_{O_2} and temperature. The reactions were written conserving Ca and Fe among the solids. The thermodynamic data (Helgeson and others, in press), reactions, and log K values used to calculate the phase boundaries shown on the diagram are listed in Appendix B while the compositional data for garnet and diopside are given in Appendix A. Log K values were calculated at P_T = 500 bars, fCO_2 = 180 bars, and at quartz and calcite saturation through the temperature range 350°-550°C.

Because Fe occurs in the oxide phase as magnetite and not hematite in the presence of quartz, limits can be placed on fO_2 and temperature in the system. These limits are represented, respectively, by the hematite - magnetite (HM) and quartz - fayalite - magnetite (QFM) buffers. Likewise, the absence of graphite in the presence of the skarn minerals was used in conjunction with maximum fCO_2 = 180 bars to calculate the CO_2 - C buffer. The conversion of calcite + quartz to wollastonite is independent of fO_2 and occurs at 540°C in the absence of Fe, and these conditions were probably met during the thermal metamorphism of the host rock which is known to locally contain only wollastonite plus calcite. However, as Fe is introduced, the reaction:

$$CaCO_3 + SiO_2 = CaSiO_3 + CO_2$$

becomes unstable, and thus it is represented as a dashed line in Figure 19.

Figure 19. Mineral stabilities among some of the phases in skarn A. -- Symbols are: H, hematite; M, magnetite; Q, quartz; Cal, calcite; woll, wollastonite. HM, hematite - magnetite buffer; QFM, quartz - fayalite - magnetite buffer. Path a→b→c→d depicts schematic evolution of mineralizing fluids. Single bar arrows indicate the direction of the expanding garnet and pyroxene fields at f_{CO_2} values less than 180 bars. Phase boundaries were calculated at a total pressure of 500 bars, at quartz and calcite saturation, and with unit activities for the solid phases.

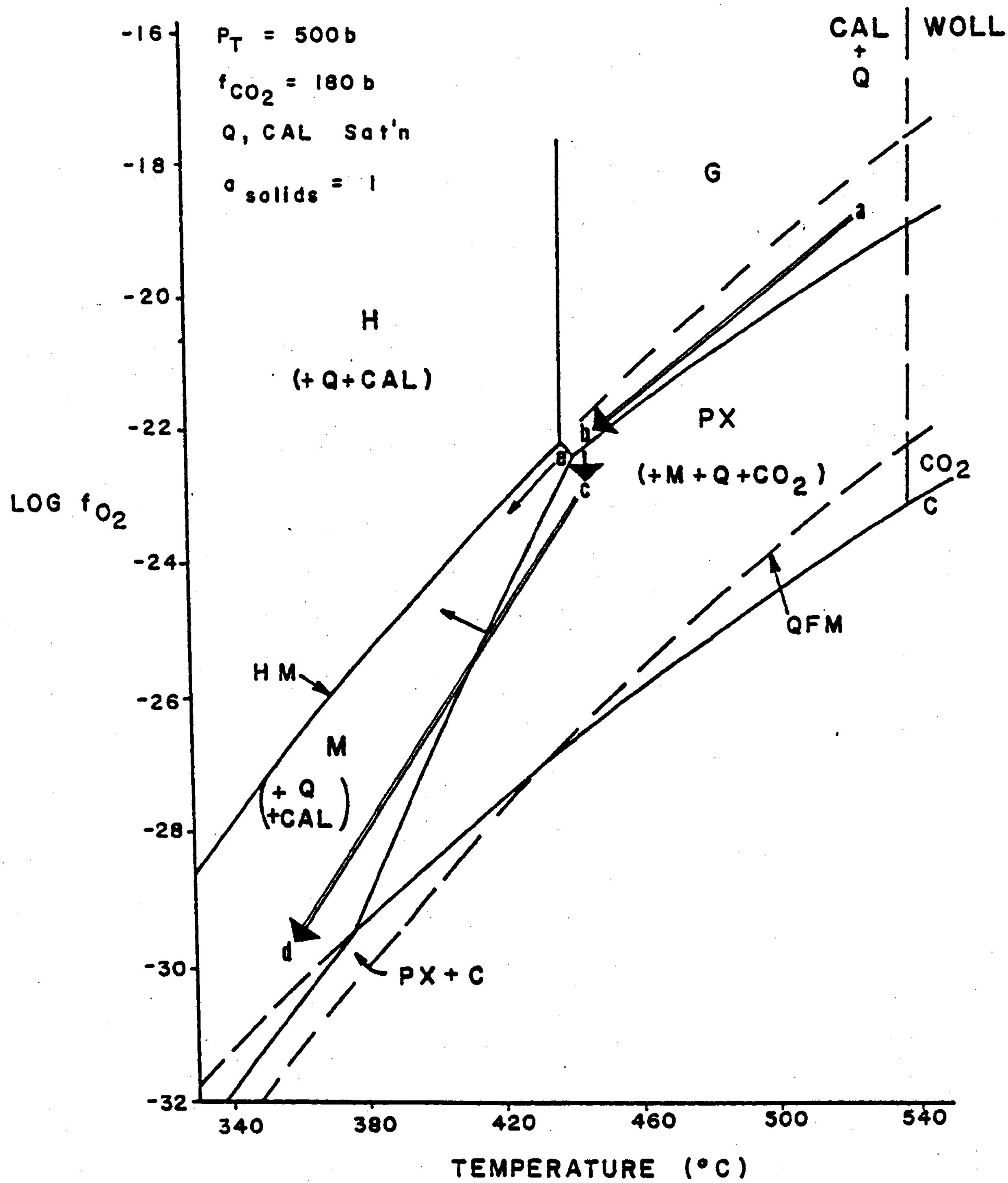

Figure 19. Mineral stabilities among some of the phases in skarn A.

From Figure 19, the following information can be deduced: 1) Garnet is stable above 440°C; 2) Pyroxene plus magnetite, in the presence of quartz, is stable at temperatures below that of the garnet stability field; and 3) Magnetite in the presence of quartz and calcite is stable below 440°C. Because paragenetic studies indicate that the contemporaneous deposition of magnetite, quartz, and pyroxene largely postdates that of garnet, and that magnetite, calcite, and quartz are deposited late (Figure 10), the chemical environment must move from the garnet stability field through the magnetite - pyroxene field to the magnetite stability field. This changing chemical environment is depicted schematically by the path a→b→c→d shown in Figure 19. At time a, and at temperatures $\geq$ 440°C, the host rock, siliceous limestone, was converted by the addition of Fe to garnet. The replacement of garnet by pyroxene suggests that the mineralizing solutions cross the garnet - pyroxene phase boundary (Point b, Figure 19). The apparent contemporaneous deposition of pyroxene, magnetite, and quartz after garnet deposition indicates that the solutions moved to the pyroxene + magnetite + quartz field (Point c, Figure 19). Finally, the late deposition of magnetite + calcite + quartz indicates that the solutions moved to point d through decreasing temperatures and fO_2 values.

The relationships shown in Figure 19 are based on a calculated maximum fCO_2 of 180 bars determined from fluid inclusion data. A minimum fCO_2 can be determined for the stable assemblage garnet + pyroxene + magnetite + quartz + calcite from the phase relationships shown in Figure 19. As fCO_2 decreases, the magnetite + calcite field collapses at the expense of the pyroxene and garnet fields, shown by the single bar arrows in Figure 19. Thus, a minimum fCO_2 value is that value at which point e will intersect the HM buffer which is approximately 96 bars. Below this value, the assemblage garnet + pyroxene + magnetite + quartz + calcite is no longer stable.

In summary, the environment of skarn formation was accompanied by decreasing temperature and fO_2 values, and thus, the theoretical thermal evolution of fluids based on paragenetically determined stable mineral assemblages agrees to within about 60°C of the thermal history ascertained from high temperature fluid inclusions in garnet and quartz. With different composition of solids and different P_{CO_2} values, the stability fields would change slightly, but the overall relationships should remain the same.

Skarn B

Paragenetic studies of skarn B indicate an initial deposition of garnet followed by replacement with fine grained diopside plus vesuvianite away from the mineralized fault that localizes the skarn. Along the fault, coarse grained diopside is sequentially replaced by vesuvianite and muscovite plus calcite. Later, manganese oxide formed as altered rims around coarse diopside grains, and pyrite and pyrrhotite were deposited in adjacent siliceous rocks. The thermal evolution of these minerals cannot be absolutely documented because only fluid inclusions in coarse diopside were determined. Diopside was precipitated from solutions with salinities that fluctuated between 44 and 50 weight percent NaCl equivalent, at temperatures between 480° and 550°C, and at a minimum pressure of 570 bars. The occurrence of calcite as a paragenetically late mineral and the absence of wollastonite indicate that temperatures probably decreased by the time calcite was deposited. Using the same limitations for skarn B as were used to determine depth to mineralization in skarn A, a minimum cover of 2000 meters is obtained (Figures 17 and 18). This agrees to within 300 meters of the minimum depth of cover over skarn A during its formation.

The chemical evolution of skarn B can be represented by the following reactions:

1) $$\underset{\text{sanidine}}{3KAlSi_3O_8} + 2H^+ = \underset{\text{muscovite}}{KAl_3Si_3O_{10}(OH)_2} = 2K^+ + \underset{\text{quartz}}{6SiO_2}$$

2) $$\underset{\text{garnet}}{3Ca_3Al_{1.4}Fe_{.6}Si_3O_{12}} + 2H_2O + Mg^{++} =$$

$$\underset{\text{vesuvianite}}{X^{+1}Ca_9Al_{4.2}Fe_{.8}Mg_{1.0}Si_9O_{34}(OH)_4} + Fe.$$

One way to get the shift in stability from sanidine to muscovite in reaction (1) is to lower the temperature of the solution with a fixed K^+/H^+ ratio (Montoya and Hemley, 1975). Reaction (2) describes the addition of H_2O and Mg^{++} to aluminous garnet, resulting in release of Fe as garnet is converted to vesuvianite. The garnet was assigned an Al/Fe ratio of about 2 because its occurrence within a calcareous bed of the Abrigo Formation and its pale green color suggest that it is grossularitic. The composition of vesuvianite was determined by microprobe analysis (Sample 67, Appendix A) normalized to 9 silicon (Deer, Howie, and Zussman, 1966). Because Na and K were not analyzed, the site occupied by Ca appears deficient which is denoted by an X in the formula for vesuvianite. Furthermore, some probe error must account for the low Ca content. Although no thermodynamic data exists for vesuvianite, reaction (2) reasonably supports the paragenetic determination of early garnet replaced by vesuvianite and accounts for the source of Fe in pyrite and pyrrhotite that occurs in surrounding siliceous rocks. The introduction of Mg^{++} is a local feature compared to the larger scale Fe metasomatism in skarn A. The interpretation of Mg^{++} metasomatism is supported by the observation that early fine grained diopside is volumetrically insignificant compared to later coarse grained diopside that forms up to 80% of the skarn near the fault. Because calcium is ubiquitous, the introduction of Mg^{++} is required to augment the volume percent of diopside initially present.

SUMMARY AND CONCLUSIONS

The geologic history in the study area began in the Precambrian with the dynamic metamorphism of Pinal Schist and intrusion of Cochise Peak Quartz Monzonite. The relative ages of these two events are not discernible from field studies. Beginning in the Middle Cambrian Period, sandstone, with a basal arkose derived from the quartz monzonite, was deposited over the quartz monzonite. During the remainder of the Paleozoic Era, a sequence of shallow marine carbonates was deposited. This stratigraphy was deformed during the Laramide orogeny (Gilluly, 1956) by a major period of folding and the apparent detachment of sedimentary rocks from basement quartz monzonite. A detachment is suggested by the observation that the contact between sedimentary rocks and quartz monzonite is almost everywhere a low angle fault. The geometric relationships of rock units within one large overturned fold permit the interpretation that sedimentary and basement (?) rocks were folded and transported to the northeast along a west dipping low angle fault. Similar fold - fault geometries are noted by Berg (1962) in the Laramide basement cored uplifts in the Rocky Mountain foreland.

During Middle Tertiary time, Stronghold Granite intruded and thermally metamorphosed the deformed country rocks. Thermal metamorphism postdates and transgresses Laramide low angle fault breccias (Gilluly, 1956) and is best displayed in the siliceous limestones of the Abrigo Formation. The purest carbonate rocks were recrystallized to marbles while the sandstones were slightly recrystallized or virtually unaffected. Thermal metamorphism of Cochise Peak Quartz Monzonite is essentially nonexistent, consistent with the fact that the quartz monzonite's mineralogy was generated at magmatic conditions. A period of high angle faulting accompanied Middle Tertiary plutonism, and the faults served to localize the intrusion of rhyolite dikes and introduction of metasomatic skarn assemblages. Crosscutting thermal metamorphic assemblages are metasomatic skarn assemblages, two of which are represented by skarns A and B.

At skarn A, early saline fluids containing ~ 40 weight percent NaCl + KCl deposited fluorite at moderately high temperatures (300°-$330^{\circ}C$) under lithostatic pressure. An increase in temperature to about $530^{\circ}C$ and decrease in salinity to less than 26.4 weight percent NaCl mark the onset of garnet deposition, and probably were attended by moderate Fe metasomatism. The subsequent deposition of diopside, chlorite, magnetite, and quartz indicates decreasing temperature and a possible change from lithostatic to hydrostatic pressure. The large volume percent of magnetite present indicates continual Fe addition. By the time late fluorite was deposited, temperatures had declined to a plateau of approximately 340°C and salinities had decreased to 1.8 weight percent NaCl indicating low salinity waters during late stages of skarn formation. Introduction of late low salinity water was facilitated by the development of intense fracturing in the host rock. Calcite deposition probably occurred at temperatures lower than those of late fluorite deposition. Finally, minor magnetite, pyrite, hematite (?) and chalcopyrite were deposited.

The evolution of skarn B is characterized by early thermal metamorphism of Abrigo limestone and siltstone with subsequent influx of H_2O, Mg^{++}, and $S^{=}$ along a low angle fault converting grossular garnet, fine grained diopside, and sanidine to coarse grained diopside, vesuvianite, muscovite, and calcite. The mineralogical differences between skarns A and B can be attributed to the kinds of metasomatism: skarn A developed through the introduction of Fe, whereas skarn B formed during contemporaneous Mg metasomatism and introduction of $S^{=}$. In skarn B, the conversion of garnet to vesuvianite was accompanied by the release of Fe which was later precipitated as pyrite and pyrrhotite in surrounding siliceous rocks. Fluid inclusions in second stage diopside record temperatures between 480° and 550°C which appear to represent the highest temperatures attained in the skarn. The late deposition of calcite, in the absence of wollastonite, suggests that temperatures decreased from the time of diopside deposition through that of calcite. Hydrolysis of ubiquitous adjacent calcite supplied the constituents for late precipitation of this phase in interstitial sites of the other skarn minerals. As in skarn A, the early solutions were highly saline, averaging 47 weight percent NaCl equivalent.

The high temperatures in both skarns A and B place restrictions on the distance between skarn and its heat source. The interpretation that the Stronghold Granite pluton is the heat source for skarn formation is substantiated by the fact that both skarns are $\leq$ 350 meters from the contact. The high temperatures indicated for garnet in skarn A are similar to those determined by Surles (1978) in garnets from Washington Camp. She concluded that garnet was formed during conductive heat transport into siliceous limestones from a cooling pluton. In skarn B, the early minerals (grossular garnet, diopside, and sanidine) could reasonably have been formed by recrystallization of Abrigo Formation during initial conductive heat transport, while vesuvianite and muscovite, minerals that require the presence of H_2O, could have formed by later convective heat transport away from a cooling pluton. Norton and Knight (1977) have modeled both types of heat transport around a cooling batholith-sized pluton intruded to a depth of ~ 2 km. The 600°C isotherm for a conductive heat transport model generally conforms to the shape of the top and sides of the pluton and occurs within a few hundred meters of the pluton for about 10^5 years (Norton and Knight, 1977, Figure 1, p. 952; Figure 3, p. 953). In a convective heat transport model, the 600°C isotherm varies in its geometrical relationship to a pluton depending upon initial rock permeabilities and the amount of time elapsed from intrusion. If both pluton and host rock are fractured, the 600°C isotherm is rapidly withdrawn from the pluton contact by 5×10^5 years after intrusion (Norton and Knight, 1977, Figure 23, p. 971). Therefore, convective heat transport may occur, but its role in the metamorphism of Abrigo limestone would have been restricted to an early period of granite crystallization immediately adjacent to the pluton.

Skarns A and B were localized by intense fracturing and faulting, respectively, at a minimum depth of 2.3 km. The formation of skarn A can be attributed to the intrusion of Stronghold Granite because of the proximity of granite to the skarn and because solution geochemistry can be interpreted to indicate that the mineralizing solutions were derived, in part, from the crystallizing pluton. However, skarn B sits closer to Cochise Peak Quartz Monzonite than to Stronghold Granite which renders the interpretation of skarn formation due to intrusion of the granite less obvious.

That the formation of skarn B is attributed to the granite heat source is based on field evidence. Cochise Peak Quartz Monzonite cannot be the heat source bacause it is older than the rocks that contain skarn mineralization. Because there is no other exposed intrusive in the vicinity of the study area which is younger than Paleozoic rocks and yet older than Stronghold Granite, the granite is the only definitive heat source. Therefore, it appears that skarn B is localized by a fault that fortuitously occurs near quartz monzonite, and like all the other skarns in the field area, its formation is attributed to intrusion of Stronghold Granite.

APPENDIX A

ELECTRON MICROPROBE METHODS AND ANALYSES OF SOME SKARN MINERALS

Electron microprobe studies were used to determine the compositions of garnet and diopside in skarn A and diopside and vesuvianite in skarn B. Assuming perfect stoichiometry for ugrandite garnet and diopside, analyses were always within $\pm$ 1.5% of the total weight percent of oxides. The analysis of vesuvianite (sample 67), however, indicates a total of 95.92 weight percent oxides. The balance of weight occurs as H_2O, and because the stoichiometry of Ca is low, probably includes small amounts of K_2O and Na_2O.

In order to calculate mineral stabilities of garnet and diopside, the mole fraction of iron in both minerals is needed. The mole fractions, listed at the end of this appendix, were calculated assuming all iron to be in the ferric and ferrous states respectively for garnet and diopside and assuming perfect stoichiometry of ugrandite garnet and diopside. The following formulas were used to determine mole fraction of the iron end member of garnet (X_{ad}) and hedenbergite (X_{hd}):

$$X_{ad} = \frac{\text{moles } Fe_2O_3}{\text{moles } Fe_2O_3 + \text{moles } Al_2O_3}$$

$$X_{hd} = \frac{\text{moles FeO}}{\text{moles FeO} + \text{moles MgO} + \text{moles MnO}}$$

Table A-1. Microprobe Analyses of Some Skarn Minerals (Weight Percent).

SAMPLE	ANALYSIS	CaO	Fe_2O_3	FeO	MgO	MnO	Al_2O_3	SiO_2	X_{ad}	X_{hd}
1	a	39.98	21.05		0.23	0.45	7.17	36.85	0.65	
	b	33.80	21.41		0.15	0.74	7.01	36.72	0.66	
	c	33.29	22.29		0.10	0.37	5.97	36.06	0.71	
2	a	31.44	26.87		0.01	2.38	3.14	34.91	0.85	
	b	32.61	28.05		0.03	0.61	2.81	35.18	0.86	
3	a	25.45		4.03	16.36	0.53	0.29	54.36		0.12
49	a	33.23	17.77		0.13	1.08	9.04	37.15	0.56	
66	a	25.66		1.33	17.81	0.66	0.28	54.89		0.04
	b	25.57		1.17	18.06	0.40	0.58	53.51		0.03
	c	25.63		0.70	18.36	0.44	0.21	55.48		0.02
67	a	35.44	4.87		3.14	0.62	14.91	36.94		

APPENDIX B

THERMODYNAMIC DATA, REACTIONS AND EQUILIBRIUM CONSTANTS USED IN DETERMINING MINERAL STABILITIES OF SKARN A

Table B-1. Thermodynamic Data for Phases Used in This Study; Data from Helgeson and Others (1978).

NAME	FORMULA	$\Delta H^o_{f,298.15}$[a]	$S^o_{298.15}$[a]	$C_p = \hat{a} + \hat{b} \times 10^{-3}T + \hat{c} \times 10^5 T^{-2}$[b]			$V^o_{298.15}$[a]
				$\hat{a}$	$\hat{b} \times 10^3$	$\hat{c} \times 10^{-5}$	
Andradite	$Ca_3Fe_2Si_3O_{12}$	-1,381,005	70.13	113.532	15.636	-30.889	131.85
Hedenbergite	$CaFeSi_2O_6$	- 678,496	40.70	54.81	8.17	-15.01	68.27
Fayalite	Fe_2SiO_4	- 354,119	35.45	36.51	9.36	- 6.70	46.39
Magnetite	Fe_3O_4	- 267,250	34.83	21.88	48.20	0	44.524
Hematite	Fe_2O_3	- 197,720	20.94	23.49	18.60	- 3.55	30.274
Quartz	SiO_2	- 217,650	9.88	11.22	8.20	- 2.70	22.688
Calcite	$CaCO_3$	- 288,772	22.15	24.98	5.24	- 6.20	36.934
Wollastonite	$CaSiO_3$	- 389,810	19.60	26.64	3.60	- 6.52	39.93
CO_2		- 94,054	51.072	10.57	2.10	- 2.06	0
O_2		0	49.003	7.16	1.0	- 0.40	0
C		0	1.372	4.03	1.14	- 2.04	5.298

Table B-2. Equilibrium Constants (Log K's) for Reactions of Minerals Used in This Study.

REACTIONS	Log K Values at 500 Bars and Indicated Temperatures in °C						
	250°	300°	350°	400°	450°	500°	550°
$2Fe_3O_4 + \frac{1}{2}O_2 = 3Fe_2O_3$	17.64	15.50	13.69	12.15	10.81	9.64	8.60
$2Fe_3O_4 + 3SiO_2 = 3Fe_2SiO_4 + O_2$	-40.11	-35.66	-31.95	-28.82	-26.15	-23.87	-21.89
$C + O_2 = CO_2$	39.45	36.02	33.13	30.68	28.56	26.72	25.10
$CaSiO_3 + CO_2 = CaCO_3 + SiO_2$	0.93	0.13	- 0.53	- 1.09	- 1.57	- 1.98	- 2.33
$Ca_3Fe_2Si_3O_{12} + 3CO_2 = 3CaCO_3 + Fe_2O_3 + 3SiO_2$	- 0.97	- 2.84	- 4.39	- 5.69	- 6.81	- 7.76	- 8.58
$3Ca_3Fe_2Si_3O_{12} + 9CO_2 = 9CaCO_3 + 2Fe_3O_4 + 9SiO_2 + \frac{1}{2}O_2$	-24.76	-29.25	-33.05	-36.30	-39.09	-41.51	-43.60
$Ca_3Fe_2Si_3O_{12} + 3CO_2 = 3CaCO_3 + Fe_2SiO_4 + 2SiO_2 + \frac{1}{2}O_2$	-20.19	-19.85	-19.55	-19.29	-19.06	-18.85	-18.66
$2CaFeSi_2O_6 + \frac{1}{2}O_2 + 2CO_2 = 2CaCO_3 + Fe_2O_3 + 4SiO_2$	19.37	15.78	12.77	10.23	8.06	6.18	4.55
$3CaFeSi_2O_6 + \frac{1}{2}O_2 + 3CO_2 = 3CaCO_3 + Fe_3O_4 + 6SiO_2$	20.23	15.92	12.32	9.28	6.68	4.45	2.52
$2CaFeSi_2O_6 + 2CO_2 = 2CaCO_3 + Fe_2SiO_4 + 3SiO_2$	0.15	- 1.24	- 2.39	- 3.36	- 4.20	- 4.91	- 5.53
$Ca_3Fe_2Si_3O_{12} + CO_2 + SiO_2 = 2CaFeSi_2O_6 + CaCO_3 + \frac{1}{2}O_2$	-20.34	-18.61	-17.16	-15.93	-14.87	-13.94	-13.13
$3CaFeSi_2O_6 + 3C + 7/2\ O_2 = Fe_3O_4 + 3CaCO_3 + 6SiO_2$	138.58	123.96	111.72	101.31	92.37	84.61	77.82

REFERENCES

Berg, R. R., 1962, Mountain flank thrusting in Rocky Mountain foreland, Wyoming and Colorado: Am. Assoc. Petroleum Geologists Bull., v. 46, p. 2019-2032.

Bodnar, R. J., 1978, Fluid inclusion study of the porphyry copper prospect at Red Mountain, Arizona: M.S. Thesis (Unpublished), Univ. of Arizona.

Brock, W. G. and Engelder, T., 1977, Deformation associated with the movement of the Muddy Mountain overthrust in the Buffington Window, southeastern Nevada: Geol. Soc. America Bull., v. 88, p. 1667-1677.

Bryant, D. L., 1968, Diagnostic characteristics of the paleozoic formations of southeastern Arizona, _in_ Southern Arizona Guidebook III, Titley, S. R., ed., Arizona Geological Society, Tucson, p. 33-48.

Buddington, A. F., 1959, Granite emplacement with special reference to North America: Geol. Soc. America Bull., v. 70, p. 671-748.

Cederstrom, D. J., 1946, The structural geology of the Dragoon Mountains, Arizona: Am. Jour. Sci., v. 244, p. 601-621.

Damon, P. E. and Bickerman, M., 1964, Potassium-argon dating of post-Laramide plutonic and volcanic rocks within the basin and range province of southeastern Arizona and adjacent areas: Arizona Geol. Soc. Digest, v. VII, p. 63-78.

Deer, W. A., Howie, R. A., and Zussman, J., 1966, An Introduction to the Rock Forming Minerals, John Wiley and Sons Inc., New York.

Ellis, A. J. and Golding, R. M., 1963, The solubility of calcite in sodium chloride solutions at high temperatures: Am. Jour. Sci., v. 261, p. 259-267.

Gilluly, J., 1956, General geology of central Cochise County, Arizona: U. S. Geol. Survey Prof. Paper 281.

Haas, J. L., Jr., 1971, The effect of salinity on the maximum thermal gradient of a hydrothermal system at hydrostatic pressure: Econ. Geol., v. 66, p. 940-946.

Helgeson, H. C., Delany, J. M., Nesbitt, H. W., and Bird, D. K., in press, Summary and critique of the thermodynamic properties of rock forming minerals: Am. Jour. Sci.

Holland, H. D., 1967, Ganque minerals in hydrothermal deposits, in Geochemistry of Hydrothermal Ore Deposits, Barnes, H. L. (ed.), Holt, Rinehart, and Winston, Inc., New York, p. 382-436.

Keith, S. B. and Barrett, L. F., 1976, Tectonics of the central Dragoon Mountains: A new outlook: Arizona Geol. Soc. Digest, v. X, p. 169-204.

Kerrick, D. M., 1977, The genesis of zoned skarns in the Sierra Nevada, California: J. Petrol., v. 18, p. 144-181.

Marvin, R. F., Stern, T. W., Creasy, S. C., and Mehnert, H. H., 1973, Radiometric ages of igneous rocks from Pima, Santa Cruz, and Cochise Counties, southern Arizona: U. S. Geol. Survey Bull. 1379.

Montoya, J. W. and Hemley, J. J., 1975, Activity relations and stabilities in alkali feldspar and mica alteration reactions: Econ. Geol., v. 70, p. 577-582.

Nash, J. T., 1976, Fluid inclusion petrology - data from porphyry copper deposits and applications to exploration: U. S. Geol. Survey Prof. Paper 907-D, p. D1-D16.

Norton, D. L. and Knight, I. E., 1977, Transport phenomena in hydrothermal systems: cooling plutons: Am. Jour. Sci., v. 277, p. 937-981.

Perry, D. V., 1964, Genesis of the contact rocks at the Abril Mine, Cochise County, Arizona: M.S. Thesis (Unpublished), Univ. of Arizona.

Potter, R. W., II, 1977, Pressure corrections for fluid inclusion homogenization temperatures based on the volumetric properties of the system $NaCl-H_2O$: U. S. Geol. Survey Jour. Research, v. 5, p. 603-607.

Potter, R. W., II, Babcock, R. S., and Brown, D. L., 1977, A new method for determining the solubility of salts in aqueous solutions at elevated temperatures: U. S. Geol. Survey Jour. Research, v. 5, p. 389-395.

Ransome, F. L., 1913, The turquoise copper mining district, Arizona: U. S. Geol. Survey Bull. 530-C, p. 125-134.

Roedder, E., 1962, Studies of fluid inclusions I: low temperature application of a dual purpose freezing and heating stage: Econ. Geol., v. 57, p. 1045-1061.

Roedder, E., 1963, Studies of fluid inclusions II: freezing data and their interpretation: Econ. Geol., v. 58, p. 167-211.

Roedder, E., 1967, Fluid inclusions as samples of ore fluids, in Geochemistry of Hydrothermal Ore Deposits, Barnes, H. L., ed., Holt, Rinehart, and Winston, Inc., New York, p. 515-574.

Roedder, E., 1971, Fluid inclusion studies on the prophyry-type ore deposits at Bingham, Utah, Butte, Montana, and Climax, Colorado: Econ. Geol., v. 66, p. 98-120.

Sourirajan, S. and Kennedy, G. C., 1962, The system H_2O-NaCl at elevated temperatures and pressures: Am. Jour. Sci., v. 260, p. 115-141.

Sousa, F. X., in preparation, Geology of the Middlemarch Mine and vicinity, central Dragoon Mountains, Cochise County, Arizona: M. S. Thesis, Univ. of Arizona.

Surles, T. L., 1978, Chemical and thermal variations accompanying formation of garnet skarns near Patagonia, Arizona: M. S. Thesis (Unpublished), Univ. of Arizona.

Takenouchi, S. and Kennedy, G. C., 1965, The solubility of carbon dioxide in NaCl solutions at high temperatures and pressures: Am. Jour. Sci., v. 263, p. 445-454.

Urusova, M. A., 1975, Volume properties of aqueous solutions of NaCl at elevated temperatures and pressures: Zh. Neogan. Khimii, v. 20, p. 3103-3110.

Wilson, E. D., 1927, Geology and ore deposits of the Courtland-Gleeson region, Arizona: Univ. of Arizona, Arizona Bureau of Mines Bull. 123.

#9/ F.P.
3065-8

EXPLANATION

CENOZOIC	QUATERNARY	Qal	Alluvium	Loosely consolidated sands and gravels
	TERTIARY	Tr	Rhyolite porphyry dikes	Pinkish brown porphyritic rhyolite; quartz and K-feldspar phenocrysts in an aphanitic groundmass; distinct blue-grey 6-10cm chill margin where intruded into Stronghold Granite
		Tl	Lamprophyre dikes	Small dikes containing fine grained amphibole and feldspar
		Ta	Aplite and quartz porphyry dikes	White, medium grained, friable aplite dikes and fine grained, dense quartz porphyry dikes; occur as apophyses of Stronghold Granite
		Tsg	Stronghold Granite	Light grey, medium grained, equigranular to porphyritic biotite granite; exfoliation surfaces common
PALEOZOIC	UPPER PALEOZOIC	UPz	Undifferentiated	Includes Escabrosa Limestone, Horquilla Formation, Earp Formation, and Colina Limestone; mapped as one unit; thick to medium bedded; white to dark grey, coarse to fine grained limestone; interbedded shale laminae and silicified sandstone (rocks mapped as Horquilla by Gilluly, 1956, contain highly silicified sandstone beds, local thin laminae of siltstones, and contorted chert beds)
	UPPER DEVONIAN	Dm	Martin Formation	Grey, fine to medium grained, medium to fine bedded limestone and a few sandstone beds; Light to rust brown, knotty weathered surfaces
	LATE CAMBRIAN	Єa	Abrigo Formation	Interbedded siltstone, shale, limestone, and dolostone; thin bedded, mottled, gnarly, and brecciated; local edgewise conglomerate; ribbed texture on weathered surfaces; white, blue-green, brown and black, depending upon composition of the rock
	MIDDLE CAMBRIAN	Єb	Bolsa Quartzite	White to pink, fine to medium grained, moderately well sorted quartzose sandstone with silica cement; locally friable and iron stained near faults; locally conglomeratic to arkosic
PRECAMBRIAN		pЄqm	Cochise Peak Quartz Monzonite	Porphyritic quartz monzonite; distinct, often lineated K-feldspar phenocrysts 2cm to 1cm; cataclastic texture common; locally mylonitic; weathered to orange-brown hummocky masses
		pЄp	Pinal Schist	Muscovite-quartz-chlorite spotted schist with crenulation cleavage
		sk	Massive skarn development	

SYMBOLS

Contact

Unconformity

Folds
showing plunge and trace of axial plane; dashed where inferred

Anticline

Syncline

Overturned anticline

Faults

Normal fault
showing dip, dashed where inferred, dotted where concealed; U, upthrown side, D, downthrown side

Low angle fault
showing dip, dashed where inferred, queried where questionable; sawteeth on hanging wall

Strike and dip of beds
inclined
vertical
overturned

Strike and dip of foliation
inclined
vertical

Portal of adit

Prospect pit

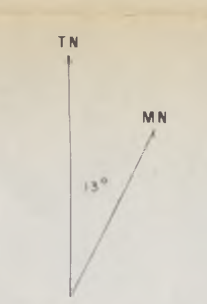

SCALE 1:3780

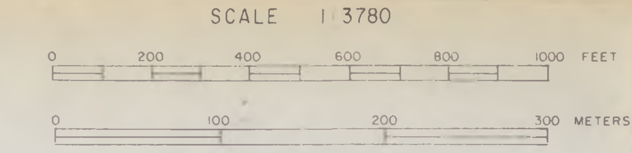

GEOLOGIC MAP OF A PORTION OF THE NORTHEAST CONTACT OF STRONGHOLD GRANITE

DRAGOON MOUNTAINS

COCHISE COUNTY, ARIZONA

FIGURE 4

J. A. Rushing, M. S. Thesis, Department of Geosciences, 1978